

Li Jun · Bao Yuchen · Hu Peng

A dynamic stiffness method for analysis of thermal effect on vibration and buckling of a laminated composite beam

Received: 17 September 2016 / Accepted: 31 March 2017 / Published online: 10 April 2017
© Springer-Verlag Berlin Heidelberg 2017

Abstract Thermal effects on vibration and buckling behaviors of generally layered composite beams with arbitrary boundary conditions are dealt with in this paper. The composite beam is modeled using third-order shear deformation beam theory in which the Poisson effect is incorporated. A constant temperature change through the beam thickness is assumed. An exact dynamic stiffness matrix is formulated by directly solving the differential equations of motion governing the natural vibration of the composite beams subjected to uniform temperature changes along the beam thickness. Application of the derived dynamic stiffness matrix together with the Wittrick–Williams algorithm to compute the natural frequencies and buckling temperature changes of two particular composite beams is discussed. The correctness and accuracy of the derived dynamic stiffness matrix is evaluated by comparing the present results with the available solutions in literature. The influences of Poisson effect, boundary condition, temperature change, thermal expansion coefficient and material anisotropy on the natural frequencies of the composite beams are studied.

Keywords Composite beams · Natural vibration · Thermal buckling · Poisson effect · Third-order shear deformation beam theory

1 Introduction

Laminated composite beams are widely used in many engineering applications owing to many advantages that they can provide: high strength-to-weight ratio, high stiffness-to-weight ratio, superior fatigue characteristics, ability to be tailored to meet the design requirements by varying the fiber orientation, material and stacking pattern [1,2]. Composite beams may be subjected to severe thermal environments, and their thermal stability is of paramount importance in specific cases [3–12,12]. Geometrically perfect composite beams generally develop compressive axial stresses due to heating or cooling and buckle at a specific temperature.

A great deal of research is devoted to analyzing the vibration and mechanical buckling behaviors of laminated composite beams. However, the existing studies on the thermal buckling of composite beams are relatively few. Kapania and Raciti [1,2] presented a review of the advances in the buckling and vibration analyses of laminated beams until 1989. Based on the first-order shear deformation theory, Mathew et al. [3] developed a one-dimensional beam finite element to investigate the thermal buckling of antisymmetric cross-ply composite beams. Lan et al. [4] developed a finite element model to explore the thermal buckling of three-layer sandwich beams with the effects of transverse shear deformation in the facings and the effects of stretching and bending deformations in the core considered. Abramovich [5] used the first-order deformation theory based on the Timoshenko-type equations to investigate the thermal buckling of cross-ply symmetric

and non-symmetric laminated composite beams. Mannini [6] studied the thermal buckling of symmetric and antisymmetric cross-ply composite beams using the first-order shear deformation theory in conjunction with the Rayleigh–Ritz method. Suresh et al. [7] proposed a semi-analytical approach to determine the nonlinear dynamic stability characteristics of asymmetrically laminated composite beams based on the first-order shear deformation theory. Lee and Choi [8] studied the thermal buckling and postbuckling behaviors of a composite beam with embedded shape memory alloy wire actuators under a uniform temperature change on the basis of the classical lamination beam theory. Khdeir [9] adopted the state space concept in conjunction with Jordan canonical form to solve exactly the thermal buckling of cross-ply laminated composite beams. Aydogdu [10] presented the thermal buckling analysis of cross-ply laminated composite beams subjected to different sets of boundary conditions. The analysis was based on a three-degree-of-freedom shear deformable beam theory, and the numerical results were obtained by the Ritz method. Pradeep et al. [11] investigated the vibration and thermal buckling behaviors of sandwich beams with composite facings and viscoelastic core. Each composite laminate was modeled as an equivalent single layer, and the transverse shear deformation was neglected. Xiang and Yang [12] investigated the free and forced vibration behaviors of a three-layer laminated functionally graded beam subjected to one-dimensional steady heat conduction in the thickness direction based on the Timoshenko beam theory and differential quadrature method. Mahi et al. [13] used an analytical method to investigate the free vibration of symmetric functionally graded beams with general boundary conditions and subjected to initial thermal stresses on the basis of a unified higher-order shear deformation beam theory. Wattanasakulpong et al. [14] adopted an improved third-order shear deformation beam theory and the Ritz method to study the thermal buckling and vibration of functionally graded beams with various immovable boundary conditions. Kiani et al. [15] studied the buckling behaviors of functionally graded material beams with surface-bonded piezoelectric layers subject to both the thermal loading and the constant voltage based on the Timoshenko beam theory. Based on the Euler–Bernoulli beam theory, Fu et al. [16] investigated the thermal buckling, nonlinear free vibration and dynamic stability of the clamped–clamped functionally graded material beam with surface-bonded piezoelectric actuators in thermal environment. Vosoughi et al. [17] presented the thermal buckling and postbuckling analysis of symmetric composite beams with temperature-dependent properties based on the first-order shear deformation beam theory and differential quadrature method. Anand Rao et al. [18] used the finite element method to study the buckling and free vibration of functionally graded beams in thermal environment based on the Timoshenko beam formulation. Fu et al. [19] presented the analytical solutions of the thermal buckling and postbuckling of symmetrically laminated beams under the uniform temperature rise on the basis of the Timoshenko beam theory. Based on the Euler–Bernoulli beam theory and Reddy beam theory, Emam and Eltahir [20] studied the hygrothermal buckling and postbuckling behaviors of composite beams whose material properties are temperature- and moisture-dependent.

A literature survey indicates that almost all of the previous studies on the thermal buckling of composite beams are focused on the cross-ply laminated beams. To the best of authors' knowledge, there is no investigation on the thermal buckling of general lay-up composite beams reported in literature. To achieve the maximum structural efficiency, it is often necessary to adopt the composite laminates with various stacking sequences. Therefore, there is a need to study the thermal buckling problem of generally layered composite beams. Furthermore, it seems that there is no work dealing with the effect of temperature change on the natural frequency of laminated composite beams.

In order to accurately and effectively predict the natural vibration and thermal buckling characteristics of generally laminated composite beams, a comprehensive structural model must be developed. It is well known that the classical beam theory with shear deformation and rotary inertia neglected overestimates the vibration frequency and buckling load of composite beams. Considering the fact that the transverse shear modulus of composite materials is much lower compared with the in-plane modulus, the shear deformation effect is taken into account in the present structural model. The material couplings among the extensional, bending and shear deformations, which are commonly present in the generally laminated composite beams, are also included in the present model. Furthermore, the Poisson effect which is often ignored in the analysis of cross-ply composite beams is incorporated in the present model for accurate prediction of the vibration and buckling characteristics of composite beams with arbitrary lay-ups.

In the present paper, the dynamic stiffness method is employed to investigate the natural vibration and thermal buckling of generally layered composite beams subjected to uniform temperature change along beam thickness for various classical boundary conditions. The third-order shear deformation beam theory [21] is used in the analysis, which assumes in-plane displacement as cubic function of thickness coordinate yielding parabolic transverse shear strain distribution through beam thickness and satisfying the strain-free conditions on the upper and lower surfaces of the beam. The coupled differential equations governing the natural vibra-

tion of generally laminated composite beams subject to uniform temperature changes are derived by use of the Hamilton’s principle. In the derivations, it is assumed that the material properties are independent of temperature, thus temperature enters the formulation only through constitutive equations. Also, the Poisson effect is accounted for in the one-dimensional beam constitutive equations. A dynamic stiffness matrix is established from the exact analytical solutions of the homogeneous differential equations of the general lay-up composite beams. Because of the use of the exact analytical solutions, the dynamic stiffness matrix describes the mass distribution within a composite beam element exactly. This property makes the dynamic stiffness method [22–24] very attractive to obtain the higher-order natural frequencies with better accuracy and reduce the computational cost when compared with the conventional finite element technique and other approximate approaches. The derived dynamic stiffness matrix in conjunction with the Wittrick–Williams algorithm [25] is used to accurately evaluate the natural frequency and critical temperature change of the composite beams. Comparisons between the present critical buckling temperatures and the available results in literature are given to demonstrate the correctness and accuracy of the proposed formulation. Natural frequencies for antisymmetric cross-ply and generally layered composite beams are also given for different boundary conditions, temperature changes, thermal expansion coefficients and material anisotropy.

2 Theoretical analysis

Consider a uniform straight laminated beam having length L , breadth b and thickness h as shown in Fig. 1. The laminated beam is made of linearly elastic orthotropic layers, and the principal material axes of each layer may be oriented at an arbitrary angle with respect to the x -axis. In the right-handed Cartesian coordinate system, the x -axis is coincident with the beam axis and the origin is in the middle plane of the beam. Only the deformation of the laminated beam in the x – z plane is considered in the present work.

The assumed displacement field for the laminated composite beam on the basis of third-order shear deformation theory [21] can be written as

$$u_1(x, z, t) = u(x, t) + z \left[\phi - \frac{4}{3} \left(\frac{z}{h} \right)^2 \left(\phi + \frac{\partial w}{\partial x} \right) \right] \tag{1a}$$

$$u_2(x, z, t) = 0 \tag{1b}$$

$$u_3(x, z, t) = w(x, t) \tag{1c}$$

where $u_1(x, z, t)$, $u_2(x, z, t)$ and $u_3(x, z, t)$ denote the displacements of any point in the laminated beam domain along the x , y and z directions, respectively. $u(x, t)$ and $w(x, t)$ represent the displacements of a point in the beam mid-plane along the x and z directions, respectively. $\phi(x, t)$ is the rotation of the section normal to the mid-plane about the y -axis, t is time.

The strain–displacement relations are obtained from the displacement field given by Eqs. (1a)–(1c)

$$\varepsilon_x = \varepsilon_x^0 + z\kappa_x^0 + z^3\kappa_x^2 \tag{2a}$$

$$\gamma_{xz} = \gamma_{xz}^0 + z^2\kappa_{xz}^2 \tag{2b}$$

where

$$\varepsilon_x^0 = \frac{\partial u}{\partial x} \quad \kappa_x^0 = \frac{\partial \phi}{\partial x} \quad \kappa_x^2 = -\frac{4}{3h^2} \left(\frac{\partial \phi}{\partial x} + \frac{\partial^2 w}{\partial x^2} \right) \tag{2c}$$

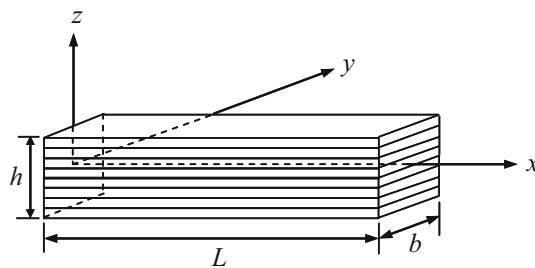


Fig. 1 Geometry of laminated beam and coordinate system

$$\gamma_{xz}^0 = \left(\phi + \frac{\partial w}{\partial x} \right) \quad \kappa_{xz}^2 = -\frac{4}{h^2} \left(\phi + \frac{\partial w}{\partial x} \right) \tag{2d}$$

It can be seen from Eqs. (2b) and (2d) that the displacement field given by Eqs. (1a)–(1c) accommodates quadratic variation of transverse shear strain (and hence stress) and vanishing of transverse shear stress on the top and bottom surfaces of the laminated beam. Thus, there is no need to use the shear correction factor.

According to the third-order shear deformation laminate theory, when the thermal effect is present, the constitutive equations of the laminated composite plate can be written as

$$\begin{Bmatrix} N_x \\ N_y \\ N_{xy} \\ M_x \\ M_y \\ M_{xy} \\ P_x \\ P_y \\ P_{xy} \end{Bmatrix} = \begin{bmatrix} A_{11} & A_{12} & A_{16} & B_{11} & B_{12} & B_{16} & E_{11} & E_{12} & E_{16} \\ A_{12} & A_{22} & A_{26} & B_{12} & B_{22} & B_{26} & E_{12} & E_{22} & E_{26} \\ A_{16} & A_{26} & A_{66} & B_{16} & B_{26} & B_{66} & E_{16} & E_{26} & E_{66} \\ B_{11} & B_{12} & B_{16} & D_{11} & D_{12} & D_{16} & F_{11} & F_{12} & F_{16} \\ B_{12} & B_{22} & B_{26} & D_{12} & D_{22} & D_{26} & F_{12} & F_{22} & F_{26} \\ B_{16} & B_{26} & B_{66} & D_{16} & D_{26} & D_{66} & F_{16} & F_{26} & F_{66} \\ E_{11} & E_{12} & E_{16} & F_{11} & F_{12} & F_{16} & H_{11} & H_{12} & H_{16} \\ E_{12} & E_{22} & E_{26} & F_{12} & F_{22} & F_{26} & H_{12} & H_{22} & H_{26} \\ E_{16} & E_{26} & E_{66} & F_{16} & F_{26} & F_{66} & H_{16} & H_{26} & H_{66} \end{bmatrix} \begin{Bmatrix} \varepsilon_x^0 \\ \varepsilon_y^0 \\ \gamma_{xy}^0 \\ \kappa_x^0 \\ \kappa_y^0 \\ \kappa_{xy}^0 \\ \kappa_x^2 \\ \kappa_y^2 \\ \kappa_{xy}^2 \end{Bmatrix} - \begin{Bmatrix} N_x^T \\ N_y^T \\ N_{xy}^T \\ M_x^T \\ M_y^T \\ M_{xy}^T \\ P_x^T \\ P_y^T \\ P_{xy}^T \end{Bmatrix} \tag{3a}$$

$$\begin{Bmatrix} Q_{yz} \\ Q_{xz} \\ R_{yz} \\ R_{xz} \end{Bmatrix} = \begin{bmatrix} A_{44} & A_{45} & D_{44} & D_{45} \\ A_{45} & A_{55} & D_{45} & D_{55} \\ D_{44} & D_{45} & F_{44} & F_{45} \\ D_{45} & D_{55} & F_{45} & F_{55} \end{bmatrix} \begin{Bmatrix} \gamma_{yz}^0 \\ \gamma_{xz}^0 \\ \kappa_{yz}^2 \\ \kappa_{xz}^2 \end{Bmatrix} \tag{3b}$$

where N_x , N_y and N_{xy} denote the in-plane forces, M_x , M_y and M_{xy} the bending and twisting moments, P_x , P_y and P_{xy} the higher-order bending and twisting moments, Q_{yz} and Q_{xz} the shear forces, R_{yz} and R_{xz} the higher-order shear forces. N_x^T , N_y^T and N_{xy}^T denote the in-plane thermal forces, M_x^T , M_y^T and M_{xy}^T the thermal bending and twisting moments, P_x^T , P_y^T and P_{xy}^T the higher-order thermal bending and twisting moments. ε_x^0 , ε_y^0 , γ_{xy}^0 , γ_{yz}^0 and γ_{xz}^0 represent the mid-plane strains, κ_x^0 , κ_y^0 and κ_{xy}^0 the bending and twisting curvatures, κ_x^2 , κ_y^2 , κ_{xy}^2 , κ_{yz}^2 and κ_{xz}^2 the higher-order bending and twisting curvatures. A_{ij} , B_{ij} , D_{ij} , E_{ij} , F_{ij} , H_{ij} ($i, j = 1, 2, 6$) and A_{ij} , D_{ij} , F_{ij} ($i, j = 4, 5$) are the laminate stiffness coefficients.

For the case of the laminated beam under consideration, its width direction is free of stresses. Therefore, the in-plane forces N_y and N_{xy} , the bending and twisting moments M_y and M_{xy} , the higher-order bending and twisting moments P_y and P_{xy} , and the shear forces Q_{yz} and R_{yz} are assumed to be equal to zero while the mid-plane strains ε_y^0 , γ_{xy}^0 and γ_{yz}^0 , the bending and twisting curvatures κ_y^0 and κ_{xy}^0 , and the higher-order bending and twisting curvatures κ_y^2 , κ_{xy}^2 and κ_{yz}^2 are assumed to be nonzero. The following constitutive equations for the laminated beam, in which the temperature effect and Poisson effect are taken into account, can be obtained from Eqs. (3a) and (3b)

$$\begin{Bmatrix} N_x \\ M_x \\ P_x \end{Bmatrix} = \begin{Bmatrix} \bar{N}_x \\ \bar{M}_x \\ \bar{P}_x \end{Bmatrix} - \begin{Bmatrix} \bar{N}_x^T \\ \bar{M}_x^T \\ \bar{P}_x^T \end{Bmatrix} \tag{4a}$$

$$\begin{Bmatrix} Q_{xz} \\ R_{xz} \end{Bmatrix} = \begin{bmatrix} \bar{A}_{55} & \bar{D}_{55} \\ \bar{D}_{55} & \bar{F}_{55} \end{bmatrix} \begin{Bmatrix} \gamma_{xz}^0 \\ \kappa_{xz}^2 \end{Bmatrix} \tag{4b}$$

where

$$\begin{Bmatrix} \bar{N}_x \\ \bar{M}_x \\ \bar{P}_x \end{Bmatrix} = \begin{bmatrix} \bar{A}_{11} & \bar{B}_{11} & \bar{E}_{11} \\ \bar{B}_{11} & \bar{D}_{11} & \bar{F}_{11} \\ \bar{E}_{11} & \bar{F}_{11} & \bar{H}_{11} \end{bmatrix} \begin{Bmatrix} \varepsilon_x^0 \\ \kappa_x^0 \\ \kappa_x^2 \end{Bmatrix} \tag{5a}$$

$$\begin{bmatrix} \bar{A}_{11} & \bar{B}_{11} & \bar{E}_{11} \\ \bar{B}_{11} & \bar{D}_{11} & \bar{F}_{11} \\ \bar{E}_{11} & \bar{F}_{11} & \bar{H}_{11} \end{bmatrix} = \begin{bmatrix} A_{11} & B_{11} & E_{11} \\ B_{11} & D_{11} & F_{11} \\ E_{11} & F_{11} & H_{11} \end{bmatrix}$$

$$- \begin{bmatrix} A_{12} & B_{12} & B_{16} & A_{16} & E_{12} & E_{16} \\ B_{12} & D_{12} & D_{16} & B_{16} & F_{12} & F_{16} \\ E_{12} & F_{12} & F_{16} & E_{16} & H_{12} & H_{16} \end{bmatrix} \begin{bmatrix} A_{22} & B_{22} & B_{26} & A_{26} & E_{22} & E_{26} \\ B_{22} & D_{22} & D_{26} & B_{26} & F_{22} & F_{26} \\ B_{26} & D_{26} & D_{66} & B_{66} & F_{26} & F_{66} \\ A_{26} & B_{26} & B_{66} & A_{66} & E_{26} & E_{66} \\ E_{22} & F_{22} & F_{26} & E_{26} & H_{22} & H_{26} \\ E_{26} & F_{26} & F_{66} & E_{66} & H_{26} & H_{66} \end{bmatrix}^{-1} \begin{bmatrix} A_{12} & B_{12} & E_{12} \\ B_{12} & D_{12} & F_{12} \\ B_{16} & D_{16} & F_{16} \\ A_{16} & B_{16} & E_{16} \\ E_{12} & F_{12} & H_{12} \\ E_{16} & F_{16} & H_{16} \end{bmatrix} \quad (5b)$$

$$\begin{Bmatrix} \bar{N}_x^T \\ \bar{M}_x^T \\ \bar{P}_x^T \end{Bmatrix} = \begin{Bmatrix} N_x^T \\ M_x^T \\ P_x^T \end{Bmatrix}$$

$$- \begin{bmatrix} A_{12} & B_{12} & B_{16} & A_{16} & E_{12} & E_{16} \\ B_{12} & D_{12} & D_{16} & B_{16} & F_{12} & F_{16} \\ E_{12} & F_{12} & F_{16} & E_{16} & H_{12} & H_{16} \end{bmatrix} \begin{bmatrix} A_{22} & B_{22} & B_{26} & A_{26} & E_{22} & E_{26} \\ B_{22} & D_{22} & D_{26} & B_{26} & F_{22} & F_{26} \\ B_{26} & D_{26} & D_{66} & B_{66} & F_{26} & F_{66} \\ A_{26} & B_{26} & B_{66} & A_{66} & E_{26} & E_{66} \\ E_{22} & F_{22} & F_{26} & E_{26} & H_{22} & H_{26} \\ E_{26} & F_{26} & F_{66} & E_{66} & H_{26} & H_{66} \end{bmatrix}^{-1} \begin{Bmatrix} N_y^T \\ M_y^T \\ M_{xy}^T \\ N_{xy}^T \\ P_y^T \\ P_{xy}^T \end{Bmatrix} \quad (5c)$$

$$\begin{bmatrix} \bar{A}_{55} & \bar{D}_{55} \\ \bar{D}_{55} & \bar{F}_{55} \end{bmatrix} = \begin{bmatrix} A_{55} & D_{55} \\ D_{55} & F_{55} \end{bmatrix} - \begin{bmatrix} D_{45} & A_{45} \\ F_{45} & D_{45} \end{bmatrix} \begin{bmatrix} F_{44} & D_{44} \\ D_{44} & A_{44} \end{bmatrix}^{-1} \begin{bmatrix} D_{45} & F_{45} \\ A_{45} & D_{45} \end{bmatrix} \quad (5d)$$

The laminate stiffness coefficients $A_{ij}, B_{ij}, D_{ij}, E_{ij}, F_{ij}, H_{ij}$ ($i, j = 1, 2, 6$) and A_{ij}, D_{ij}, F_{ij} ($i, j = 4, 5$) appearing in Eqs. (3a) and (3b) are defined in terms of the transformed reduced stiffness constants \bar{Q}_{ij} as follows

$$(A_{ij} \ B_{ij} \ D_{ij} \ E_{ij} \ F_{ij} \ H_{ij}) = \int_{-\frac{h}{2}}^{\frac{h}{2}} \bar{Q}_{ij} (1 \ z \ z^2 \ z^3 \ z^4 \ z^6) dz \quad (i, j = 1, 2, 6) \quad (6a)$$

$$(A_{ij} \ D_{ij} \ F_{ij}) = \int_{-\frac{h}{2}}^{\frac{h}{2}} \bar{Q}_{ij} (1 \ z^2 \ z^4) dz \quad (i, j = 4, 5) \quad (6b)$$

The thermal forces and moments appearing in Eq. (3a) can be expressed as

$$\begin{Bmatrix} N_x^T \\ N_y^T \\ N_{xy}^T \end{Bmatrix} = \int_{-\frac{h}{2}}^{\frac{h}{2}} \begin{bmatrix} \bar{Q}_{11} & \bar{Q}_{12} & \bar{Q}_{16} \\ \bar{Q}_{12} & \bar{Q}_{22} & \bar{Q}_{26} \\ \bar{Q}_{16} & \bar{Q}_{26} & \bar{Q}_{66} \end{bmatrix} \begin{Bmatrix} \alpha_x \Delta T \\ \alpha_y \Delta T \\ 2\alpha_{xy} \Delta T \end{Bmatrix} dz \quad (7a)$$

$$\begin{Bmatrix} M_x^T \\ M_y^T \\ M_{xy}^T \end{Bmatrix} = \int_{-\frac{h}{2}}^{\frac{h}{2}} \begin{bmatrix} \bar{Q}_{11} & \bar{Q}_{12} & \bar{Q}_{16} \\ \bar{Q}_{12} & \bar{Q}_{22} & \bar{Q}_{26} \\ \bar{Q}_{16} & \bar{Q}_{26} & \bar{Q}_{66} \end{bmatrix} z \begin{Bmatrix} \alpha_x \Delta T \\ \alpha_y \Delta T \\ 2\alpha_{xy} \Delta T \end{Bmatrix} dz \quad (7b)$$

$$\begin{Bmatrix} P_x^T \\ P_y^T \\ P_{xy}^T \end{Bmatrix} = \int_{-\frac{h}{2}}^{\frac{h}{2}} \begin{bmatrix} \bar{Q}_{11} & \bar{Q}_{12} & \bar{Q}_{16} \\ \bar{Q}_{12} & \bar{Q}_{22} & \bar{Q}_{26} \\ \bar{Q}_{16} & \bar{Q}_{26} & \bar{Q}_{66} \end{bmatrix} z^3 \begin{Bmatrix} \alpha_x \Delta T \\ \alpha_y \Delta T \\ 2\alpha_{xy} \Delta T \end{Bmatrix} dz \quad (7c)$$

where α_x, α_y and α_{xy} are the transformed thermal coefficients of the laminate, which are defined in the ‘‘Appendix.’’ ΔT is a constant temperature change from a reference state.

The transformed reduced stiffness constants \bar{Q}_{ij} ($i, j = 1, 2, 6$) and \bar{Q}_{ij} ($i, j = 4, 5$) are given in the ‘‘Appendix.’’

The strain energy of the laminated composite beam shown in Fig. 1 can be written as

$$V = \frac{1}{2} \int_0^L (\bar{N}_x \varepsilon_x^0 + \bar{M}_x \kappa_x^0 + \bar{P}_x \kappa_x^2 + Q_{xz} \gamma_{xz}^0 + R_{xz} \kappa_{xz}^2) b dx \quad (8a)$$

Substituting Eqs. (2c) and (2d) into Eq. (8a), one obtains

$$V = \frac{1}{2} \int_0^L \left[\bar{N}_x \frac{\partial u}{\partial x} + \bar{M}_x \frac{\partial \phi}{\partial x} - \bar{P}_x \frac{4}{3h^2} \left(\frac{\partial \phi}{\partial x} + \frac{\partial^2 w}{\partial x^2} \right) + Q_{xz} \left(\phi + \frac{\partial w}{\partial x} \right) - R_{xz} \frac{4}{h^2} \left(\phi + \frac{\partial w}{\partial x} \right) \right] b dx \quad (8b)$$

The kinetic energy of the laminated composite beam can be expressed as

$$T = \frac{1}{2} \int_0^L \int_{-\frac{h}{2}}^{\frac{h}{2}} \rho \left[\left(\frac{\partial u_1}{\partial t} \right)^2 + \left(\frac{\partial u_2}{\partial t} \right)^2 + \left(\frac{\partial u_3}{\partial t} \right)^2 \right] b dz dx \quad (9a)$$

where ρ is the mass density of the lamina material.

Introduction of Eqs. (1a)–(1c) into Eq. (9a) results in

$$T = \frac{1}{2} \int_0^L \left[I_1 \dot{u}^2 + I_3 \dot{\phi}^2 + \frac{16}{9h^4} I_7 \left(\dot{\phi} + \frac{\partial \dot{w}}{\partial x} \right)^2 + 2I_2 \dot{u} \dot{\phi} - \frac{8}{3h^2} I_4 \dot{u} \left(\dot{\phi} + \frac{\partial \dot{w}}{\partial x} \right) \right] b dx \quad (9b)$$

where the overdots represent the partial differentiation with respect to the time t , and

$$(I_1 \ I_2 \ I_3 \ I_4 \ I_5 \ I_7) = \int_{-\frac{h}{2}}^{\frac{h}{2}} \rho (1 \ z \ z^2 \ z^3 \ z^4 \ z^6) dz \quad (9c)$$

The work W_e done by the external load of the laminated composite beam is given by

$$W_e = \frac{1}{2} \int_0^L \bar{N}_x^T \left(\frac{\partial w}{\partial x} \right)^2 b dx \quad (10)$$

The Hamilton's principle is employed to derive the governing equations of motion and the related boundary conditions of the laminated composite beam:

$$\delta \int_{t_1}^{t_2} (T - V + W_e) dt = 0 \quad (11)$$

$\delta u = \delta w = \delta \phi = \delta w' = 0$ at $t = t_1, t_2$

where δ denotes the first variation, t_1 and t_2 are two arbitrary time instants, the superscript prime denotes the partial differentiation with the coordinate x .

Inserting Eqs. (8b), (9b) and (10) together with Eqs. (2c)–(2d), (4b) and (5a)–(5d) into Eq. (11), integrating by parts and noting that the variation must vanish leads the following governing equations of motion of the laminated composite beam

$$-I_1 \ddot{u} + \frac{4}{3h^2} I_4 \ddot{w}' - \left(I_2 - \frac{4}{3h^2} I_4 \right) \ddot{\phi} + \bar{A}_{11} u'' + \left(\bar{B}_{11} - \frac{4}{3h^2} \bar{E}_{11} \right) \phi'' - \frac{4}{3h^2} \bar{E}_{11} w''' = 0 \quad (12a)$$

$$\begin{aligned} & -\frac{4}{3h^2} I_4 \dot{u}' + \frac{16}{9h^4} I_7 \dot{w}'' - I_1 \ddot{w} + \left(\frac{16}{9h^4} I_7 - \frac{4}{3h^2} I_5 \right) \ddot{\phi}' + \frac{4}{3h^2} \bar{E}_{11} u''' - \frac{16}{9h^4} \bar{H}_{11} w'''' \\ & + \left(\frac{4}{3h^2} \bar{F}_{11} - \frac{16}{9h^4} \bar{H}_{11} \right) \phi''' + \left(\bar{A}_{55} - \frac{8}{h^2} \bar{D}_{55} + \frac{16}{h^4} \bar{F}_{55} \right) (\phi' + w'') - \bar{N}_x^T w'' = 0 \end{aligned} \quad (12b)$$

$$\begin{aligned} & -\left(I_2 - \frac{4}{3h^2} I_4 \right) \ddot{u} - \left(\frac{16}{9h^4} I_7 - \frac{4}{3h^2} I_5 \right) \ddot{w}' - \left(I_3 + \frac{16}{9h^4} I_7 - \frac{8}{3h^2} I_5 \right) \ddot{\phi} \\ & + \left(\bar{B}_{11} - \frac{4}{3h^2} \bar{E}_{11} \right) u'' + \left(\bar{D}_{11} - \frac{8}{3h^2} \bar{F}_{11} + \frac{16}{9h^4} \bar{H}_{11} \right) \phi'' - \left(\frac{4}{3h^2} \bar{F}_{11} - \frac{16}{9h^4} \bar{H}_{11} \right) w'' \\ & - \left(\bar{A}_{55} - \frac{8}{h^2} \bar{D}_{55} + \frac{16}{h^4} \bar{F}_{55} \right) (\phi + w') = 0 \end{aligned} \quad (12c)$$

and the appropriate boundary conditions at the laminated beam ends ($x = 0, L$) are

$$\left[\bar{A}_{11}u' + \left(\bar{B}_{11} - \frac{4}{3h^2}\bar{E}_{11} \right) \phi' - \frac{4}{3h^2}\bar{E}_{11}w'' \right] \delta u = 0 \quad (13a)$$

$$\left[\frac{4}{3h^2}I_4\ddot{u} - \frac{16}{9h^4}I_7\ddot{w}' - \left(\frac{16}{9h^4}I_7 - \frac{4}{3h^2}I_5 \right) \ddot{\phi} - \frac{4}{3h^2}\bar{E}_{11}u'' + \frac{16}{9h^4}\bar{H}_{11}w''' \right. \\ \left. - \left(\frac{4}{3h^2}\bar{F}_{11} - \frac{16}{9h^4}\bar{H}_{11} \right) \phi'' - \left(\bar{A}_{55} - \frac{8}{h^2}\bar{D}_{55} + \frac{16}{h^4}\bar{F}_{55} \right) (\phi + w') + \bar{N}_x^T w' \right] \delta w = 0 \quad (13b)$$

$$\left[- \left(\bar{B}_{11} - \frac{4}{3h^2}\bar{E}_{11} \right) u' - \left(\bar{D}_{11} - \frac{8}{3h^2}\bar{F}_{11} + \frac{16}{9h^4}\bar{H}_{11} \right) \phi' + \left(\frac{4}{3h^2}\bar{F}_{11} - \frac{16}{9h^4}\bar{H}_{11} \right) w'' \right] \delta \phi = 0 \quad (13c)$$

$$\left[\frac{4}{3h^2}\bar{E}_{11}u' + \left(\frac{4}{3h^2}\bar{F}_{11} - \frac{16}{9h^4}\bar{H}_{11} \right) \phi' - \frac{16}{9h^4}\bar{H}_{11}w'' \right] \delta w' = 0 \quad (13d)$$

3 Dynamic stiffness method

For the case of undamped natural vibration, it can be seen that Eqs. (12a)–(12c) have solutions that are separable in time and space and that the time dependence is harmonic. Letting

$$\{ u(x, t) \ w(x, t) \ \phi(x, t) \} = \{ U(x) \ W(x) \ \Phi(x) \} e^{i\omega t} \quad (14)$$

where ω is the circular frequency, $U(x)$, $W(x)$ and $\Phi(x)$ are the mode shapes of the harmonically varying axial displacement, bending displacement and normal rotation, respectively.

Substituting Eq. (14) into Eqs. (12a)–(12c) results in the following ordinary differential equations

$$I_1\omega^2U - \left(\frac{4}{3h^2}I_4 - I_2 \right) \omega^2\Phi - \frac{4}{3h^2}I_4\omega^2W' + \bar{A}_{11}U'' + \left(\bar{B}_{11} - \frac{4}{3h^2}\bar{E}_{11} \right) \Phi'' - \frac{4}{3h^2}\bar{E}_{11}W''' = 0 \quad (15a)$$

$$I_1\omega^2W + \frac{4}{3h^2}I_4\omega^2U' - \left(\frac{16}{9h^4}I_7 - \frac{4}{3h^2}I_5 \right) \omega^2\Phi' - \frac{16}{9h^4}I_7\omega^2W'' + \frac{4}{3h^2}\bar{E}_{11}U''' \\ + \left(\frac{4}{3h^2}\bar{F}_{11} - \frac{16}{9h^4}\bar{H}_{11} \right) \Phi''' - \frac{16}{9h^4}\bar{H}_{11}W'''' + \left(\bar{A}_{55} - \frac{8}{h^2}\bar{D}_{55} + \frac{16}{h^4}\bar{F}_{55} \right) (\Phi' + W'') - \bar{N}_x^T W'' = 0 \quad (15b)$$

$$\left(I_2 - \frac{4}{3h^2}I_4 \right) \omega^2U + \left(I_3 + \frac{16}{9h^4}I_7 - \frac{8}{3h^2}I_5 \right) \omega^2\Phi - \left(\frac{4}{3h^2}I_5 - \frac{16}{9h^4}I_7 \right) \omega^2W' \\ + \left(\bar{B}_{11} - \frac{4}{3h^2}\bar{E}_{11} \right) U'' + \left(\bar{D}_{11} - \frac{8}{3h^2}\bar{F}_{11} + \frac{16}{9h^4}\bar{H}_{11} \right) \Phi'' \\ + \left(\frac{16}{9h^4}\bar{H}_{11} - \frac{4}{3h^2}\bar{F}_{11} \right) W''' + \left(\frac{8}{h^2}\bar{D}_{55} - \bar{A}_{55} - \frac{16}{h^4}\bar{F}_{55} \right) (\Phi + W') = 0 \quad (15c)$$

The solutions to Eqs. (15a)–(15c) can be expressed as

$$\{ U(x) \ W(x) \ \Phi(x) \} = \{ \tilde{A} \ \tilde{B} \ \tilde{C} \} e^{\kappa x} \quad (16)$$

Introducing Eq. (16) into Eqs. (15a)–(15c) obtains a set of algebraic equations. Letting the determinant of the coefficient matrix of \tilde{A} , \tilde{B} and \tilde{C} equal to zero produces the characteristics equation, which is an eighth-order polynomial equation in κ :

$$\eta_4\kappa^8 + \eta_3\kappa^6 + \eta_2\kappa^4 + \eta_1\kappa^2 + \eta_0 = 0 \quad (17)$$

where the coefficients η_k ($k = 0 - 4$) are listed in the ‘‘Appendix.’’

Equation (17) can be reduced to a fourth-order polynomial equation

$$\chi^4 + a_1\chi^3 + a_2\chi^2 + a_3\chi + a_4 = 0 \quad (18a)$$

where

$$\chi = \kappa^2 \quad a_1 = \frac{\eta_3}{\eta_4} \quad a_2 = \frac{\eta_2}{\eta_4} \quad a_3 = \frac{\eta_1}{\eta_4} \quad a_4 = \frac{\eta_0}{\eta_4} \tag{18b}$$

The solutions to Eq. (18a) can be found in closed-form [26].

Equations (15a)–(15c) are a set of linear homogeneous ordinary differential equations with constant coefficients, the general solutions to which can be written as

$$\begin{aligned} U(x) &= A_1 e^{\kappa_1 x} + A_2 e^{-\kappa_1 x} + A_3 e^{\kappa_2 x} + A_4 e^{-\kappa_2 x} + A_5 e^{\kappa_3 x} + A_6 e^{-\kappa_3 x} + A_7 e^{\kappa_4 x} + A_8 e^{-\kappa_4 x} \\ &= \sum_{j=1}^4 (A_{2j-1} e^{\kappa_j x} + A_{2j} e^{-\kappa_j x}) \end{aligned} \tag{19a}$$

$$\begin{aligned} W(x) &= B_1 e^{\kappa_1 x} + B_2 e^{-\kappa_1 x} + B_3 e^{\kappa_2 x} + B_4 e^{-\kappa_2 x} + B_5 e^{\kappa_3 x} + B_6 e^{-\kappa_3 x} + B_7 e^{\kappa_4 x} + B_8 e^{-\kappa_4 x} \\ &= \sum_{j=1}^4 (B_{2j-1} e^{\kappa_j x} + B_{2j} e^{-\kappa_j x}) \end{aligned} \tag{19b}$$

$$\begin{aligned} \Phi(x) &= C_1 e^{\kappa_1 x} + C_2 e^{-\kappa_1 x} + C_3 e^{\kappa_2 x} + C_4 e^{-\kappa_2 x} + C_5 e^{\kappa_3 x} + C_6 e^{-\kappa_3 x} + C_7 e^{\kappa_4 x} + C_8 e^{-\kappa_4 x} \\ &= \sum_{j=1}^4 (C_{2j-1} e^{\kappa_j x} + C_{2j} e^{-\kappa_j x}) \end{aligned} \tag{19c}$$

where $\kappa_j = \sqrt{\chi_j}$ ($j = 1 - 4$). $A_1 - A_8$, $B_1 - B_8$ and $C_1 - C_8$ are three sets of eight constants, which are dependent. Substituting Eqs. (19a)–(19c) into Eqs. (15a) and (15b) obtains the following relations between the constants

$$A_{2j-1} = t_j C_{2j-1} \quad A_{2j} = t_j C_{2j} \tag{20a}$$

$$B_{2j-1} = \bar{t}_j C_{2j-1} \quad B_{2j} = -\bar{t}_j C_{2j} \tag{20b}$$

where

$$\begin{aligned} t_j &= \left(\left(-3 \left(3\bar{B}_{11} \left(16\bar{F}_{55} - 8\bar{D}_{55}h^2 + h^4 \left(\bar{A}_{55} - \bar{N}_x^T \right) \right) + 4\bar{E}_{11}h^2\bar{N}_x^T \right) \kappa_j^4 \right. \right. \\ &\quad - 16 \left(\bar{E}_{11}\bar{F}_{11} - \bar{B}_{11}\bar{H}_{11} \right) \kappa_j^6 + \kappa_j^2 \left(-144\bar{F}_{55}I_2 + 3h^2 \left(4\bar{E}_{11}I_1 + 24\bar{D}_{55}I_2 \right. \right. \\ &\quad - 3h^2 \left(\bar{B}_{11}I_1 + \bar{A}_{55}I_2 \right) + \left. \left. \left(3h^2I_2 - 4I_4 \right) \bar{N}_x^T \right) + 16 \left(\bar{H}_{11}I_2 - \bar{F}_{11}I_4 \right. \right. \\ &\quad \left. \left. - \bar{E}_{11}I_5 + \bar{B}_{11}I_7 \right) \kappa_j^2 \right) \omega^2 - \left(9h^4I_1I_2 - 12h^2I_1I_4 + 16 \left(I_4I_5 - I_2I_7 \right) \kappa_j^2 \right) \omega^4 \right) / \Delta_j \end{aligned} \tag{20c}$$

$$\begin{aligned} \bar{t}_j &= - \left(\kappa_j \left(4 \left(\bar{E}_{11}\kappa_j^2 + I_4\omega^2 \right) \left(4\bar{E}_{11}\kappa_j^2 - 3\bar{B}_{11}h^2\kappa_j^2 + \left(-3h^2I_2 + 4I_4 \right) \omega^2 \right) \right. \right. \\ &\quad + \left(\bar{A}_{11}\kappa_j^2 + I_1\omega^2 \right) \left(144\bar{F}_{55} - 72\bar{D}_{55}h^2 + 9\bar{A}_{55}h^4 + 4 \left(3\bar{F}_{11}h^2 - 4\bar{H}_{11} \right) \kappa_j^2 \right. \\ &\quad \left. \left. + 4 \left(3h^2I_5 - 4I_7 \right) \omega^2 \right) \right) / \Delta_j \end{aligned} \tag{20d}$$

$$\begin{aligned} \Delta_j &= \left(16 \left(\bar{E}_{11}\kappa_j^3 + I_4\kappa_j\omega^2 \right)^2 + \left(\bar{A}_{11}\kappa_j^2 + I_1\omega^2 \right) \left(9 \left(16\bar{F}_{55} - 8\bar{D}_{55}h^2 \right. \right. \right. \\ &\quad \left. \left. + h^4 \left(\bar{A}_{55} - \bar{N}_x^T \right) \right) \kappa_j^2 - 16\bar{H}_{11}\kappa_j^4 + \left(9h^4I_1 - 16I_7\kappa_j^2 \right) \omega^2 \right) \end{aligned} \tag{20e}$$

It can be seen from Eqs. (20a) and (20b), only eight of the twenty-four constants are independent. It may be noted that if any of the χ_j 's are zero or are repeated in the solution of Eq. (18a), Eqs. (19a)–(19c) must be modified according to the well-known technique of ordinary differential equations with constant coefficients, for those particular values of χ_j .

Following the sign convention established in Fig. 2, the expressions of normal force $N(x)$, shear force $S(x)$, bending moment $M(x)$ and higher-order bending moment $P(x)$ can be derived from Eqs. (13a)–(13d) and Eqs. (19a)–(19c) with the help of Eqs. (20a) and (20b)

$$N(x) = \sum_{j=1}^4 \left[\bar{A}_{11}\kappa_j t_j - \left(\frac{4}{3h^2} \bar{E}_{11} - \bar{B}_{11} \right) \kappa_j - \frac{4}{3h^2} \bar{E}_{11}\kappa_j^2 \bar{t}_j \right] \left(C_{2j-1} e^{\kappa_j x} - C_{2j} e^{-\kappa_j x} \right) \tag{21a}$$

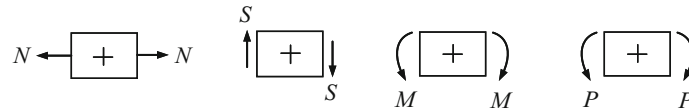


Fig. 2 Sign convention for positive normal force $N(x)$, shear force $S(x)$, bending moment $M(x)$ and higher-order bending moment $P(x)$



Fig. 3 Boundary conditions for generalized displacements and generalized forces of laminated beam

$$\begin{aligned}
 S(x) = \sum_{j=1}^4 & \left[-\frac{4}{3h^2} I_4 \omega^2 t_j + \left(-\frac{4}{3h^2} I_5 + \frac{16}{9h^4} I_7 \right) \omega^2 + \frac{16}{9h^4} I_7 \omega^2 \kappa_j \bar{t}_j \right. \\
 & - \frac{4}{3h^2} \bar{E}_{11} \kappa_j^2 t_j + \left(\frac{16}{9h^4} \bar{H}_{11} - \frac{4}{3h^2} \bar{F}_{11} \right) \kappa_j^2 + \frac{16}{9h^4} \bar{H}_{11} \kappa_j^3 \bar{t}_j \\
 & \left. + \left(\frac{8}{h^2} \bar{D}_{55} - \bar{A}_{55} - \frac{16}{h^4} \bar{F}_{55} \right) (1 + \kappa_j \bar{t}_j) + \bar{N}_x^T \kappa_j \bar{t}_j \right] (C_{2j-1} e^{\kappa_j x} + C_{2j} e^{-\kappa_j x}) \quad (21b)
 \end{aligned}$$

$$\begin{aligned}
 M(x) = \sum_{j=1}^4 & \left[\left(\frac{4}{3h^2} \bar{E}_{11} - \bar{B}_{11} \right) \kappa_j t_j + \left(\frac{8}{3h^2} \bar{F}_{11} - \bar{D}_{11} - \frac{16}{9h^4} \bar{H}_{11} \right) \kappa_j \right. \\
 & \left. + \left(\frac{4}{3h^2} \bar{F}_{11} - \frac{16}{9h^4} \bar{H}_{11} \right) \kappa_j^2 \bar{t}_j \right] (C_{2j-1} e^{\kappa_j x} - C_{2j} e^{-\kappa_j x}) \quad (21c)
 \end{aligned}$$

$$P(x) = \sum_{j=1}^4 \left[\frac{4}{3h^2} \bar{E}_{11} \kappa_j t_j + \left(\frac{4}{3h^2} \bar{F}_{11} - \frac{16}{9h^4} \bar{H}_{11} \right) \kappa_j - \frac{16}{9h^4} \bar{H}_{11} \kappa_j^2 \bar{t}_j \right] (C_{2j-1} e^{\kappa_j x} - C_{2j} e^{-\kappa_j x}) \quad (21d)$$

Referring to Fig. 3, the boundary conditions for the generalized displacements and generalized forces of the laminated composite beam can be written as

$$x = 0 : U = U_1 \quad W = W_1 \quad \Phi = \Phi_1 \quad W' = W'_1 \quad (22a)$$

$$x = L : U = U_2 \quad W = W_2 \quad \Phi = \Phi_2 \quad W' = W'_2 \quad (22b)$$

$$x = 0 : N = -N_1 \quad S = S_1 \quad M = M_1 \quad P = P_1 \quad (22c)$$

$$x = L : N = N_2 \quad S = -S_2 \quad M = -M_2 \quad P = -P_2 \quad (22d)$$

Introducing Eqs. (22a) and (22b) into Eqs. (19a)–(19c) and considering Eqs. (20a) and (20b), the nodal displacement vector $\{D\}$ can be expressed in terms of the constant vector $\{C\}$

$$\{D\} = [R]\{C\} \quad (23)$$

where

$$\{D\} = \{U_1 \quad W_1 \quad \Phi_1 \quad W'_1 \quad U_2 \quad W_2 \quad \Phi_2 \quad W'_2\}^T$$

$$\{C\} = \{C_1 \quad C_3 \quad C_5 \quad C_7 \quad C_2 \quad C_4 \quad C_6 \quad C_8\}^T$$

$$[R] = \begin{bmatrix} t_1 & t_2 & t_3 & t_4 & \bar{t}_1 & \bar{t}_2 & \bar{t}_3 & \bar{t}_4 \\ \bar{t}_1 & \bar{t}_2 & \bar{t}_3 & \bar{t}_4 & -\bar{t}_1 & -\bar{t}_2 & -\bar{t}_3 & -\bar{t}_4 \\ 1 & 1 & 1 & 1 & 1 & 1 & 1 & 1 \\ \kappa_1 \bar{t}_1 & \kappa_2 \bar{t}_2 & \kappa_3 \bar{t}_3 & \kappa_4 \bar{t}_4 & \kappa_1 \bar{t}_1 & \kappa_2 \bar{t}_2 & \kappa_3 \bar{t}_3 & \kappa_4 \bar{t}_4 \\ t_1 e^{\kappa_1 L} & t_2 e^{\kappa_2 L} & t_3 e^{\kappa_3 L} & t_4 e^{\kappa_4 L} & t_1 e^{-\kappa_1 L} & t_2 e^{-\kappa_2 L} & t_3 e^{-\kappa_3 L} & t_4 e^{-\kappa_4 L} \\ \bar{t}_1 e^{\kappa_1 L} & \bar{t}_2 e^{\kappa_2 L} & \bar{t}_3 e^{\kappa_3 L} & \bar{t}_4 e^{\kappa_4 L} & -\bar{t}_1 e^{-\kappa_1 L} & -\bar{t}_2 e^{-\kappa_2 L} & -\bar{t}_3 e^{-\kappa_3 L} & -\bar{t}_4 e^{-\kappa_4 L} \\ e^{\kappa_1 L} & e^{\kappa_2 L} & e^{\kappa_3 L} & e^{\kappa_4 L} & e^{-\kappa_1 L} & e^{-\kappa_2 L} & e^{-\kappa_3 L} & e^{-\kappa_4 L} \\ \kappa_1 \bar{t}_1 e^{\kappa_1 L} & \kappa_2 \bar{t}_2 e^{\kappa_2 L} & \kappa_3 \bar{t}_3 e^{\kappa_3 L} & \kappa_4 \bar{t}_4 e^{\kappa_4 L} & \kappa_1 \bar{t}_1 e^{-\kappa_1 L} & \kappa_2 \bar{t}_2 e^{-\kappa_2 L} & \kappa_3 \bar{t}_3 e^{-\kappa_3 L} & \kappa_4 \bar{t}_4 e^{-\kappa_4 L} \end{bmatrix}$$

Substituting Eqs. (22c) and (22d) into Eqs. (21a)–(21d), the nodal force vector $\{F\}$ corresponding to the nodal displacement vector $\{D\}$ can also be written in terms of the constant vector $\{C\}$

$$\{F\} = [H]\{C\} \tag{24}$$

where

$$\{F\} = \{N_1 \ S_1 \ M_1 \ P_1 \ N_2 \ S_2 \ M_2 \ P_2\}^T$$

$$[H] = \begin{bmatrix} -\hat{t}_1 & -\hat{t}_2 & -\hat{t}_3 & -\hat{t}_4 & \hat{t}_1 & \hat{t}_2 & \hat{t}_3 & \hat{t}_4 \\ \tilde{t}_1 & \tilde{t}_2 & \tilde{t}_3 & \tilde{t}_4 & \bar{t}_1 & \bar{t}_2 & \bar{t}_3 & \bar{t}_4 \\ \bar{\tilde{t}}_1 & \bar{\tilde{t}}_2 & \bar{\tilde{t}}_3 & \bar{\tilde{t}}_4 & -\bar{\tilde{t}}_1 & -\bar{\tilde{t}}_2 & -\bar{\tilde{t}}_3 & -\bar{\tilde{t}}_4 \\ \hat{\tilde{t}}_1 & \hat{\tilde{t}}_2 & \hat{\tilde{t}}_3 & \hat{\tilde{t}}_4 & -\hat{\tilde{t}}_1 & -\hat{\tilde{t}}_2 & -\hat{\tilde{t}}_3 & -\hat{\tilde{t}}_4 \\ \hat{t}_1 e^{\kappa_1 L} & \hat{t}_2 e^{\kappa_2 L} & \hat{t}_3 e^{\kappa_3 L} & \hat{t}_4 e^{\kappa_4 L} & -\hat{t}_1 e^{-\kappa_1 L} & -\hat{t}_2 e^{-\kappa_2 L} & -\hat{t}_3 e^{-\kappa_3 L} & -\hat{t}_4 e^{-\kappa_4 L} \\ -\tilde{t}_1 e^{\kappa_1 L} & -\tilde{t}_2 e^{\kappa_2 L} & -\tilde{t}_3 e^{\kappa_3 L} & -\tilde{t}_4 e^{\kappa_4 L} & -\tilde{t}_1 e^{-\kappa_1 L} & -\tilde{t}_2 e^{-\kappa_2 L} & -\tilde{t}_3 e^{-\kappa_3 L} & -\tilde{t}_4 e^{-\kappa_4 L} \\ -\bar{\tilde{t}}_1 e^{\kappa_1 L} & -\bar{\tilde{t}}_2 e^{\kappa_2 L} & -\bar{\tilde{t}}_3 e^{\kappa_3 L} & -\bar{\tilde{t}}_4 e^{\kappa_4 L} & \bar{\tilde{t}}_1 e^{-\kappa_1 L} & \bar{\tilde{t}}_2 e^{-\kappa_2 L} & \bar{\tilde{t}}_3 e^{-\kappa_3 L} & \bar{\tilde{t}}_4 e^{-\kappa_4 L} \\ -\hat{\tilde{t}}_1 e^{\kappa_1 L} & -\hat{\tilde{t}}_2 e^{\kappa_2 L} & -\hat{\tilde{t}}_3 e^{\kappa_3 L} & -\hat{\tilde{t}}_4 e^{\kappa_4 L} & \hat{\tilde{t}}_1 e^{-\kappa_1 L} & \hat{\tilde{t}}_2 e^{-\kappa_2 L} & \hat{\tilde{t}}_3 e^{-\kappa_3 L} & \hat{\tilde{t}}_4 e^{-\kappa_4 L} \end{bmatrix}$$

in which

$$\begin{aligned} \hat{t}_j &= \bar{A}_{11} \kappa_j t_j - \left(\frac{4}{3h^2} \bar{E}_{11} - \bar{B}_{11} \right) \kappa_j - \frac{4}{3h^2} \bar{E}_{11} \kappa_j^2 \bar{t}_j \\ \tilde{t}_j &= -\frac{4}{3h^2} I_4 \omega^2 t_j + \left(-\frac{4}{3h^2} I_5 + \frac{16}{9h^4} I_7 \right) \omega^2 + \frac{16}{9h^4} I_7 \omega^2 \kappa_j \bar{t}_j - \frac{4}{3h^2} \bar{E}_{11} \kappa_j^2 t_j + \bar{N}_x^T \kappa_j \bar{t}_j \\ &\quad + \left(\frac{16}{9h^4} \bar{H}_{11} - \frac{4}{3h^2} \bar{F}_{11} \right) \kappa_j^2 + \frac{16}{9h^4} \bar{H}_{11} \kappa_j^3 \bar{t}_j + \left(\frac{8}{h^2} \bar{D}_{55} - \bar{A}_{55} - \frac{16}{h^4} \bar{F}_{55} \right) (1 + \kappa_j \bar{t}_j) \\ \bar{\tilde{t}}_j &= \left(\frac{4}{3h^2} \bar{E}_{11} - \bar{B}_{11} \right) \kappa_j t_j + \left(\frac{8}{3h^2} \bar{F}_{11} - \bar{D}_{11} - \frac{16}{9h^4} \bar{H}_{11} \right) \kappa_j + \left(\frac{4}{3h^2} \bar{F}_{11} - \frac{16}{9h^4} \bar{H}_{11} \right) \kappa_j^2 \bar{t}_j \\ \hat{\tilde{t}}_j &= \frac{4}{3h^2} \bar{E}_{11} \kappa_j t_j + \left(\frac{4}{3h^2} \bar{F}_{11} - \frac{16}{9h^4} \bar{H}_{11} \right) \kappa_j - \frac{16}{9h^4} \bar{H}_{11} \kappa_j^2 \bar{t}_j \quad (j = 1 - 4) \end{aligned}$$

The relationship between the nodal force vector $\{F\}$ and the nodal displacement vector $\{D\}$ can be obtained by eliminating the constant vector $\{C\}$ from Eqs. (23) and (24), which produces the dynamic stiffness equation

$$\{F\} = [K]\{D\} \tag{25}$$

where $[K] = [H][R]^{-1}$ is the exact dynamic stiffness matrix, which is frequency-dependent. It should be mentioned that although the explicit analytical expressions for the elements of the dynamic stiffness matrix may be determined in partitioned form using the symbolic manipulator software such as Mathematica [27], they are too lengthy to list in the paper.

Having obtained the dynamic stiffness matrix, it can be directly applied to calculate the natural frequencies, thermal buckling loads and mode shapes of a laminated composite beam with various boundary conditions or a structure composed of such beams. An accurate, reliable and efficient method to obtain the natural frequencies and buckling loads of the laminated beam structure using the dynamic stiffness technique is to apply the Wittrick–Williams algorithm [25] which has been discussed and utilized in a number of papers [23] and is not reiterated here for brevity. The algorithm uses the Sturm sequence property of the dynamic stiffness matrix and ensures that there is no possibility of missing an eigenvalue (i.e., natural frequency in the natural vibration problem, or buckling load in the buckling problem) of the structure.

4 Numerical examples

In order to demonstrate the correctness and accuracy of the proposed dynamic stiffness formulation for the analysis of natural vibration and thermal buckling behaviors of laminated composite beams, two illustrative examples including a cross-ply composite beam and a generally laminated composite beam subjected to a constant temperature change through beam thickness are investigated.

Two classical boundary conditions at each end of the composite beams ($x = 0, L$) are considered, which are given as follows

For the clamped boundary (C): $U = W = \Phi = W' = 0$

For the hinged boundary (H): $U = W = M = P = 0$

The first example is a two-layer antisymmetric cross-ply $[0^\circ/90^\circ]$ composite beam having a rectangular cross section. All the details about the geometric properties of the beam and the material properties of each lamina used here are given below

$$E_1 = 138 \times 10^9 \text{ Pa} \quad E_2 = 6.9 \times 10^9 \text{ Pa} \quad G_{12} = G_{13} = 4.14 \times 10^9 \text{ Pa} \quad G_{23} = 3.45 \times 10^9 \text{ Pa}$$

$$\nu_{12} = 0.25 \quad \rho = 1550.1 \text{ kg/m}^3 \quad L = 0.381 \text{ m} \quad h = 0.0381 \text{ m}$$

$$\alpha_1 = 6 \times 10^{-6} 1/^\circ\text{C} \quad \alpha_2 = 18 \times 10^{-6} 1/^\circ\text{C}$$

Numerical results are given for the cross-ply composite beam for different temperature changes, different boundary conditions and different thermal expansion coefficients. The Poisson effect is also discussed. This example is chosen because of some available results in the previous studies [9,10].

In order to see the influences of temperature change and boundary condition on the natural frequencies of the cross-ply composite beam, three different temperature changes (i.e., $\Delta T = 0^\circ\text{C}$, $\Delta T = 100^\circ\text{C}$ and $\Delta T = -100^\circ\text{C}$) and three different boundary conditions (i.e., C–C, C–H and H–H) are considered in this example. For various boundary conditions, the first six natural frequencies of the cross-ply composite beam with no temperature change ($\Delta T = 0^\circ\text{C}$), temperature rise ($\Delta T = 100^\circ\text{C}$) and temperature fall ($\Delta T = -100^\circ\text{C}$) are shown in Tables 1 and 2. The natural frequencies are calculated by using the derived dynamic stiffness formulation and discretizing the whole beam with one element. In order to demonstrate the accuracy of the present formulation, the natural frequencies of the cross-ply composite beam with $\Delta T = 0^\circ\text{C}$ are also calculated by the general purpose finite element code ANSYS. The element type selected in calculating the natural frequencies in ANSYS is a layered solid element SOLID191, which is defined by 20 nodes having three degrees of freedom per node. The element mesh used in the ANSYS model is 80 divisions along x direction, eight divisions along y direction and 1 division along z direction. For the clamped end, all degrees of freedom are constrained to zero at all nodes on the end surface. For the hinged end, all degrees of freedom are constrained to zero only at nodes on the line of intersection between beam mid-plane and end surface. The first six natural frequencies of the cross-ply composite beam vibrating in the oxz plane obtained by ANSYS are also given in Table 1. The ANSYS results are taken as a reference for the evaluation of the accuracy of the present formulation. The percentage errors, shown in Table 1, are calculated by using ANSYS results as baseline.

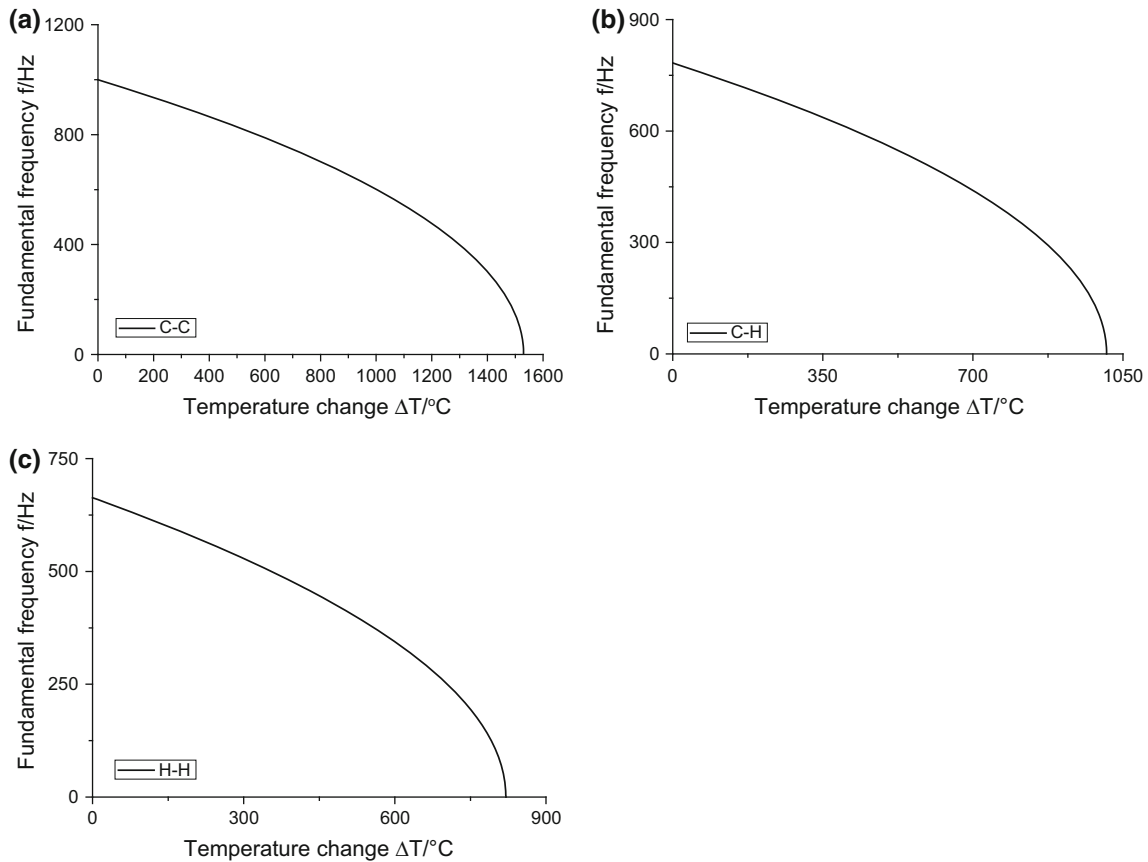
Table 1 shows that the present results are in good agreement with the ANSYS results. The natural frequencies predicted by the present formulation are generally on the higher side of the ANSYS results. The maximum percentage differences in the first six natural frequencies obtained by the present formulation for the C–C, C–H and H–H boundary conditions are 7.4, 7.0 and 8.6%, respectively, as compared to the ANSYS results. It can also be found from Tables 1 and 2 that the temperature change has a significant effect on the lower natural frequencies of the cross-ply composite beam. Also, the effect of temperature change on the higher natural frequencies is

Table 1 Natural frequencies (in Hz) of cross-ply composite beam with $\Delta T = 0^\circ\text{C}$

Mode no.	C–C			C–H			H–H		
	Present	%Error	ANSYS	Present	%Error	ANSYS	Present	%Error	ANSYS
1	999.6	1.6	983.4	783.1	1.5	771.3	663.4	2.8	645.3
2	2426.4	3.2	2350.7	2139.4	2.8	2081.2	1756.8	2.0	1723.1
3	4211.9	4.7	4023.6	3905.8	4.3	3744.4	3663.7	4.4	3510.6
4	6207.6	6.1	5853.4	5867.8	5.6	5558.3	5391.3	4.9	5137.3
5	8353.5	7.4	7779.0	7615.2	4.2	7307.8	7176.9	8.6	6606.1
6	8430.1	-1.4	8552.9	8198.1	7.0	7663.1	7804.1	7.3	7272.9

Table 2 Natural frequencies (in Hz) of cross-ply composite beam with $\Delta T = 100^\circ\text{C}$ and $\Delta T = -100^\circ\text{C}$

Mode no.	$\Delta T = 100^\circ\text{C}$			$\Delta T = -100^\circ\text{C}$		
	C-C	C-H	H-H	C-C	C-H	H-H
1	968.1	744.5	621.7	1030.0	819.7	702.5
2	2379.2	2088.5	1698.6	2472.6	2189.1	1813.1
3	4154.2	3845.6	3600.8	4268.8	3964.9	3725.6
4	6139.5	5800.4	5328.2	6274.9	5934.1	5452.9
5	8274.9	7593.6	7164.2	8430.5	7633.5	7190.1
6	8429.6	8135.3	7723.2	8431.4	8263.5	7884.1

**Fig. 4** Variation of fundamental frequency of cross-ply composite beam with temperature rise for **a** C–C, **b** C–H, **c** H–H boundary conditions

marginal. The percentage differences between the fundamental frequencies of the cross-ply composite beam with temperature rise ($\Delta T = 100^\circ\text{C}$) and the ones without temperature change for the C–C, C–H and H–H boundary conditions are -3.2 , -4.9 and -6.3% , respectively. Similarly, the percentage differences between the fundamental frequencies of the cross-ply composite beam with temperature fall ($\Delta T = -100^\circ\text{C}$) and the ones without temperature change for the C–C, C–H and H–H boundary conditions are 3.0 , 4.7 and 5.9% , respectively. For the cross-ply composite beam under study it is obvious that a temperature rise tends to decrease all of the natural frequencies, whereas a temperature fall increases them. Furthermore, a temperature rise has a more remarkable effect on the natural frequencies than the equal temperature fall. Tables 1 and 2 also show that among all of the boundary conditions the effect of temperature change on the natural frequencies is the most important for the H–H boundary condition and the least pronounced for the C–C boundary condition.

Next, the variation of the fundamental natural frequency of the cross-ply composite beam with the variation of the temperature rise is considered. Figure 4a–c shows the variation of the fundamental frequency with the temperature rise for the C–C, C–H and H–H boundary conditions, respectively.

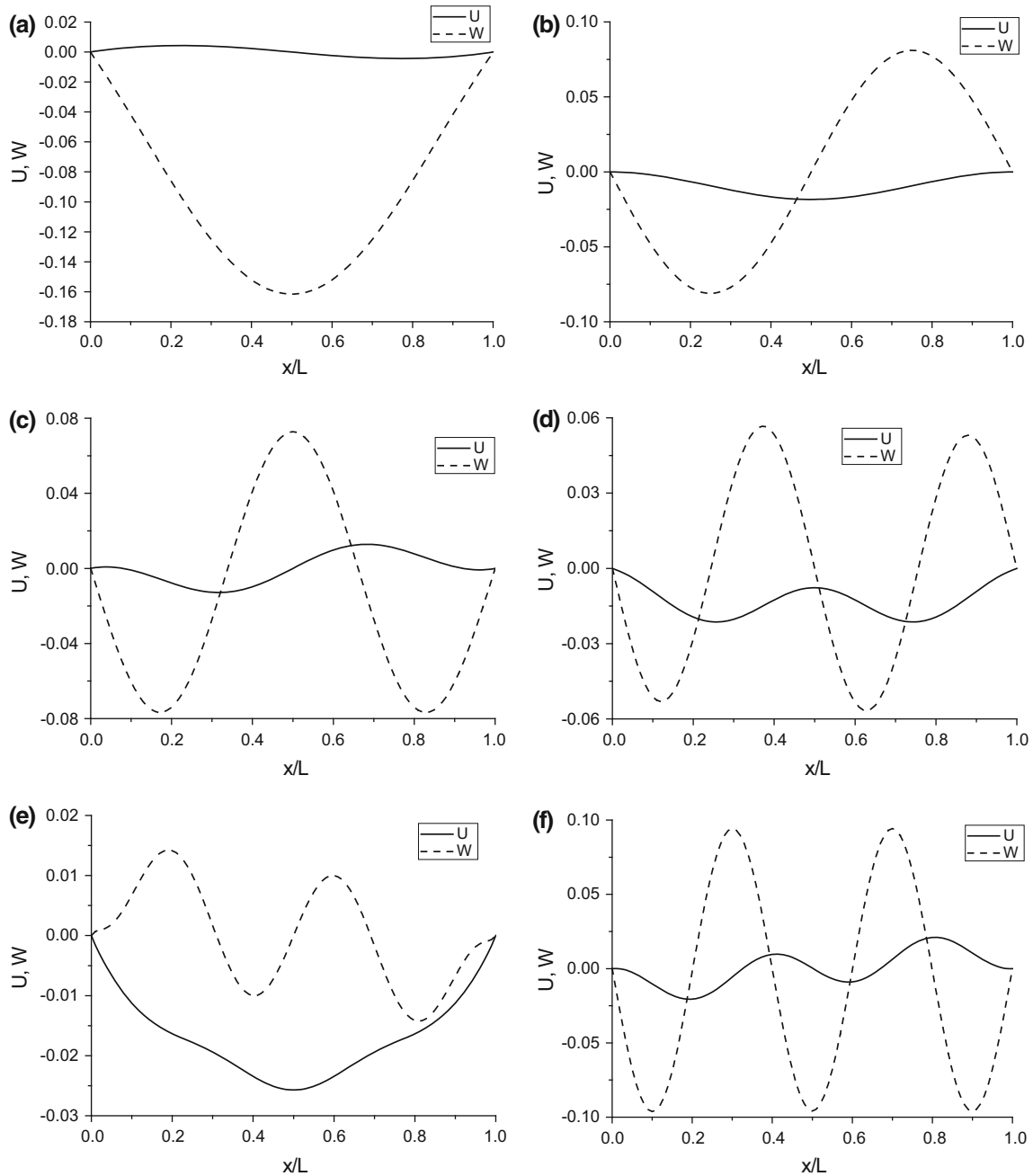


Fig. 5 First six mode shapes of the H–H cross-ply composite beam with $\Delta T = 820^\circ\text{C}$: **a** mode 1; **b** mode 2; **c** mode 3; **d** mode 4; **e** mode 5; **f** mode 6

It can be observed from Fig. 4 that the variation in the fundamental natural frequency due to the temperature rise is significant. The fundamental frequency decreases with the increase of the temperature rise, as expected. Finally at about $\Delta T = 1530.1, 1011.9$ and 820.4°C for the C–C, C–H and H–H boundary conditions, respectively, the fundamental frequency becomes zero which means that at this level of temperature rise, thermal buckling of the cross-ply composite beam occurs as a degenerate case of natural vibration at zero frequency.

The first six mode shapes of the H–H cross-ply composite beam with $\Delta T = 820^\circ\text{C}$, which is very close to the critical temperature change $\Delta T_{cr} = 820.4^\circ\text{C}$, are calculated by the present formulation and are illustrated in Fig. 5. It may be mentioned that the first six natural frequencies of the H–H cross-ply composite beam with $\Delta T = 820^\circ\text{C}$ are 14.6, 1197.7, 3109.9, 4828.8, 7079.7 and 7112.4 Hz, respectively.

Table 3 Natural frequencies (in Hz) of cross-ply composite beam without Poisson effect

Mode no.	$\Delta T = 0^\circ\text{C}$			$\Delta T = 100^\circ\text{C}$			$\Delta T = -100^\circ\text{C}$		
	C-C	C-H	H-H	C-C	C-H	H-H	C-C	C-H	H-H
1	1000.1	783.6	663.9	967.5	743.6	620.7	1031.6	821.5	704.4
2	2427.4	2140.5	1757.8	2378.6	2087.7	1697.5	2475.2	2191.9	1816.1
3	4213.3	3907.3	3665.4	4153.5	3845.0	3600.2	4272.3	3968.6	3729.4
4	6209.3	5869.8	5393.8	6138.8	5800.0	5328.3	6279.1	5938.6	5457.6
5	8355.4	7620.3	7181.5	8274.0	7597.7	7168.3	8436.1	7639.4	7195.0
6	8437.0	8200.9	7806.4	8436.5	8136.0	7722.6	8437.5	8268.4	7889.2

Table 4 Natural frequencies (in Hz) of cross-ply composite beam ($\alpha_2 = 60 \times 10^{-6}1/^\circ\text{C}$)

Mode no.	$\Delta T = 0^\circ\text{C}$			$\Delta T = 100^\circ\text{C}$			$\Delta T = -100^\circ\text{C}$		
	C-C	C-H	H-H	C-C	C-H	H-H	C-C	C-H	H-H
1	999.6	783.1	663.4	957.3	731.1	607.2	1039.9	831.6	715.1
2	2426.4	2139.4	1756.8	2363.3	2071.2	1678.7	2487.7	2205.4	1831.5
3	4211.9	3905.8	3663.7	4134.7	3825.4	3579.6	4287.6	3984.5	3746.0
4	6207.6	5867.8	5391.3	6116.6	5777.7	5306.8	6297.2	5956.0	5473.1
5	8353.5	7615.2	7176.9	8248.5	7585.6	7160.0	8430.7	7639.1	7194.6
6	8430.1	8198.1	7804.1	8429.4	8115.0	7696.1	8457.2	8285.6	7910.5

Figure 5 shows that the axial displacement and transverse displacement are coupled for all the six mode shapes. For the first mode, this coupling is rather weak. However, for the fifth mode, this coupling is rather strong.

To show the Poisson effect on the natural frequencies of the cross-ply composite beam, the first six natural frequencies of the same composite beam without the Poisson effect included are calculated and the results are displayed in Table 3. Again, three different temperature changes and three different boundary conditions are considered. It may be mentioned that if the Poisson effect is ignored, the quantities \bar{A}_{11} , \bar{B}_{11} , \bar{D}_{11} , \bar{E}_{11} , \bar{F}_{11} , \bar{H}_{11} , \bar{A}_{55} , \bar{D}_{55} , \bar{F}_{55} and \bar{N}_x^T appearing in the governing differential equations of motion and boundary conditions should be replaced by the quantities A_{11} , B_{11} , D_{11} , E_{11} , F_{11} , H_{11} , A_{55} , D_{55} , F_{55} and N_x^T .

Tables 1, 2 and 3 show that all of the natural frequencies of the cross-ply composite beam with the Poisson effect ignored are almost the same as those with the Poisson effect considered, which implies that for the cross-ply composite beam the accuracy lost in the natural frequency obtained by excluding the Poisson effect is insignificant. However, this is not the case for the generally layered composite beam, as will be shown later.

To see the effect of thermal expansion coefficient on the natural frequency of the cross-ply composite beam, α_2 varies from $\alpha_2 = 18 \times 10^{-6}1/^\circ\text{C}$ to $\alpha_2 = 60 \times 10^{-6}1/^\circ\text{C}$ while the other material properties keep the same. Three different temperature changes (namely, $\Delta T = 0^\circ\text{C}$, $\Delta T = 100^\circ\text{C}$ and $\Delta T = -100^\circ\text{C}$) and three different boundary conditions (namely, C-C, C-H and H-H) are considered. The first six natural frequencies of the cross-ply composite beam are shown in Table 4.

Tables 1, 2 and 4 clearly show that the variation of α_2 has drastic effect on the natural frequencies of the cross-ply composite beam. In addition, Tables 1, 2 and 4 show clearly that when the temperature rises, the increase of α_2 results in the decrease of the natural frequencies for all the boundary conditions. Also, Tables 1, 2 and 4 indicate that when the temperature falls, the larger the value of α_2 is, the higher the natural frequencies will be.

In order to validate the proposed dynamic stiffness formulation, it is used to evaluate the critical temperature change of the cross-ply composite beam with two different values of α_2 (namely, $\alpha_2 = 18 \times 10^{-6}1/^\circ\text{C}$ and $\alpha_2 = 60 \times 10^{-6}1/^\circ\text{C}$). The critical temperature changes obtained by the present formulation are displayed in Table 5 and compared with some available results in the literature [9, 10].

It can be found from Table 5 that the present results generally are in good agreement with the available results. The maximum percent differences between the present results and the available results in the literature [9, 10] are 3.7 and 6.3% for the cases of $\alpha_2 = 18 \times 10^{-6}1/^\circ\text{C}$ and $\alpha_2 = 60 \times 10^{-6}1/^\circ\text{C}$, respectively. The reasons for the differences are that different beam theories, constitutive equations, and solution methods are used in the present study and the literature [9, 10]. The first-order shear deformation beam theory (FOBT) and third-order shear deformation beam theory (HOBT) are used in the literature [9], in which the shear correction factor for the FOBT is set equal to 5/6. The exponential shear deformation beam theory (ESDBT) is used in the

Table 5 Buckling temperature changes (°C) of cross-ply composite beam

Boundary condition	$\alpha_2 = 18 \times 10^{-6} 1/^\circ\text{C}$				$\alpha_2 = 60 \times 10^{-6} 1/^\circ\text{C}$			
	Present	FOBT [9]	HOBT [9]	ESDBT [10]	Present	FOBT [9]	HOBT [9]	ESDBT [10]
C–C	1530.1	1496.0	1542.8	1475.0	1147.6	1147.0	1182.8	1080.0
C–H	1011.9	N/A	N/A	N/A	759.0	N/A	N/A	N/A
H–H	820.4	N/A	N/A	N/A	615.3	N/A	N/A	N/A

Table 6 frequencies (in Hz) of composite beam with $\Delta T = 0^\circ\text{C}$

Mode no.	C–C			C–H			H–H		
	Present	%Error	ANSYS	Present	%Error	ANSYS	Present	%Error	ANSYS
1	807.9	0.9%	800.3	580.7	2.7%	565.3	386.9	0	387.0
2	2009.6	0.7%	1996.2	1724.4	3.5%	1666.8	1437.2	8.4%	1326.4
3	3544.2	0.6%	3524.3	3249.8	1.9%	3188.9	2947.3	5.1%	2804.3
4	4271.3	N/A	N/A	4266.6	N/A	N/A	4252.5	N/A	N/A
5	5278.1	0.6%	5248.9	5008.3	0.9%	4965.9	4735.3	3.1%	4591.4
6	7138.6	0.6%	7098.3	6893.2	2.4%	6732.4	6637.9	2.3%	6490.4

literature [10]. The beam theory adopted in the present study is the same as the third-order shear deformation beam theory in the literature [9]. The constitutive equations used in the literature [9, 10] do not consider the Poisson effect. However, the Poisson effect is considered in the present study. Although the Poisson effect may be ignored for the cross-ply composite beam, it does have minor influence on the critical buckling temperature. As for the solution method, the state space concept in conjunction with Jordan canonical form is used in the literature [9], and the Ritz method with algebraic polynomial trial functions, which is an approximate solution method, is used in the literature [10]. The exact dynamic stiffness method in conjunction with the Wittrick–Williams algorithm is used to evaluate the natural frequency and critical temperature change in the present study.

Table 5 shows that the critical temperature change obtained by the present formulation lies between the results obtained by the FOBT [9] and HOBT [9]. Also, the critical temperature changes predicted by the present formulation is on the higher side as compared to the results predicted by the ESDBT [10]. For the case of $\alpha_2 = 18 \times 10^{-6} 1/^\circ\text{C}$ the present result is closer to the HOBT solution, while for the case of $\alpha_2 = 60 \times 10^{-6} 1/^\circ\text{C}$ the present result is in excellent agreement with the FOBT solution. As stated previously, the effect of increasing the value of α_2 is to decrease the critical temperature change of the cross-ply composite beam under considered. Increasing the value of α_2 from $18 \times 10^{-6} 1/^\circ\text{C}$ to $60 \times 10^{-6} 1/^\circ\text{C}$ decreases the critical temperature change of the C–C cross-ply composite beam by approximately 25%.

Now, consider a generally layered composite beam. The ply-stacking sequence used is $[30^\circ/50^\circ/30^\circ/50^\circ]$. The following geometric properties of the beam and material properties of each layer are used in the analysis.

$$E_1 = 138 \times 10^9 \text{ Pa} \quad E_2 = 6.9 \times 10^9 \text{ Pa} \quad G_{12} = G_{13} = 4.14 \times 10^9 \text{ Pa} \quad G_{23} = 3.45 \times 10^9 \text{ Pa}$$

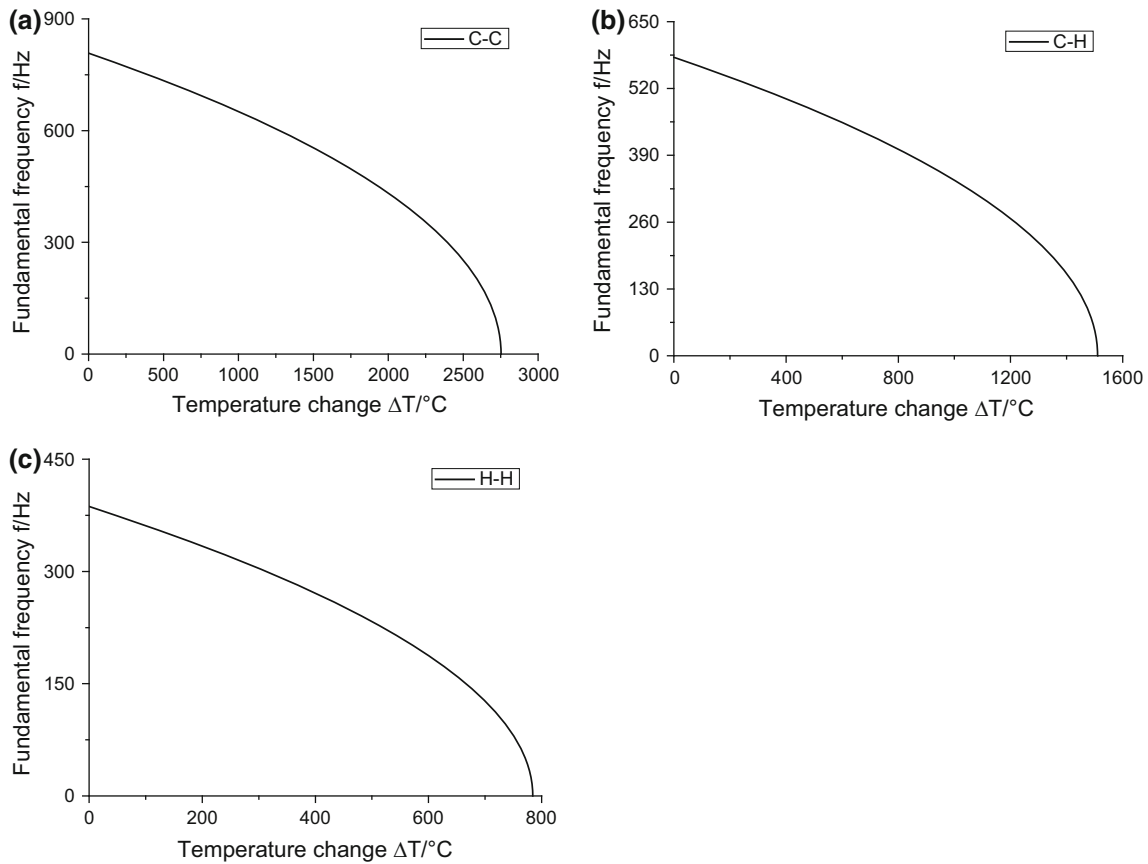
$$\nu_{12} = 0.25 \quad \rho = 1550.1 \text{ kg/m}^3 \quad L = 0.381 \text{ m} \quad h = 0.0381 \text{ m}$$

$$\alpha_1 = 6 \times 10^{-6} 1/^\circ\text{C} \quad \alpha_2 = 18 \times 10^{-6} 1/^\circ\text{C}$$

The first six natural frequencies of the composite beam with various boundary conditions are calculated using the proposed dynamic stiffness formulation, and the numerical results are presented in Tables 6 and 7, in which three different temperature changes (i.e., $\Delta T = 0^\circ\text{C}$, $\Delta T = 180^\circ\text{C}$ and $\Delta T = -180^\circ\text{C}$) are considered. The natural frequencies are obtained by idealizing the whole beam with single element. The natural frequencies of the composite beam with $\Delta T = 0^\circ\text{C}$ are also calculated by the finite element software ANSYS. The element type and mesh division used in computing the natural frequencies in ANSYS are the same as those used in the cross-ply composite beam. The first five natural frequencies of the composite beam vibrating in the oxz plane obtained by ANSYS are also shown in Table 6. It should be noted that the fourth natural frequency obtained by the present formulation, which is a predominant longitudinal vibration frequency, is not captured by ANSYS solutions. The reason for this is perhaps that the longitudinal displacement and boundary condition of the beam are difficult to model using three-dimensional solid element. The ANSYS solutions are

Table 7 Natural frequencies (in Hz) of composite beam with $\Delta T = 180^\circ\text{C}$ and $\Delta T = -180^\circ\text{C}$

Mode no.	$\Delta T = 180^\circ\text{C}$			$\Delta T = -180^\circ\text{C}$		
	C-C	C-H	H-H	C-C	C-H	H-H
1	782.4	546.0	339.6	832.6	613.3	429.0
2	1972.4	1682.8	1389.4	2046.0	1765.0	1483.5
3	3499.7	3202.4	2896.0	3588.2	3296.6	2997.7
4	4271.3	4266.3	4250.8	4271.4	4266.9	4254.0
5	5226.3	4954.8	4680.8	5329.3	5061.3	4789.5
6	7079.6	6832.8	6575.9	7197.1	6953.0	6699.2

**Fig. 6** Variation of fundamental frequency of composite beam with temperature rise for **a** C-C, **b** C-H, **c** H-H boundary conditions

regarded as a reference for the evaluation of the accuracy of the present formulation. The percentage errors shown in Table 6 are calculated by using the ANSYS solutions as baseline.

As can be observed from Table 6, the natural frequencies predicted by the present formulation are also found to be in good agreement with the ANSYS solutions. The natural frequencies produced by the present formulation are also on the higher side of the ANSYS solutions. Tables 6 and 7 clearly show that for the case of temperature rise, the lower natural frequencies decrease with fast rate and the higher natural frequencies decrease with slow rate. Similarly, for the case of temperature fall, the lower natural frequencies increase with fast rate and the higher natural frequencies increase with slow rate. The influence of temperature change on the much higher natural frequencies is practically negligible. In addition, Tables 6 and 7 show that the temperature change has virtually no influence on the fourth natural frequency of the C-C, C-H and H-H composite beam because these frequencies correspond to the modes with predominance of longitudinal vibrations. Moreover, Tables 6 and 7 clearly show that the H-H composite beam yields the lowest natural frequency and the C-C composite beam produces the highest one.

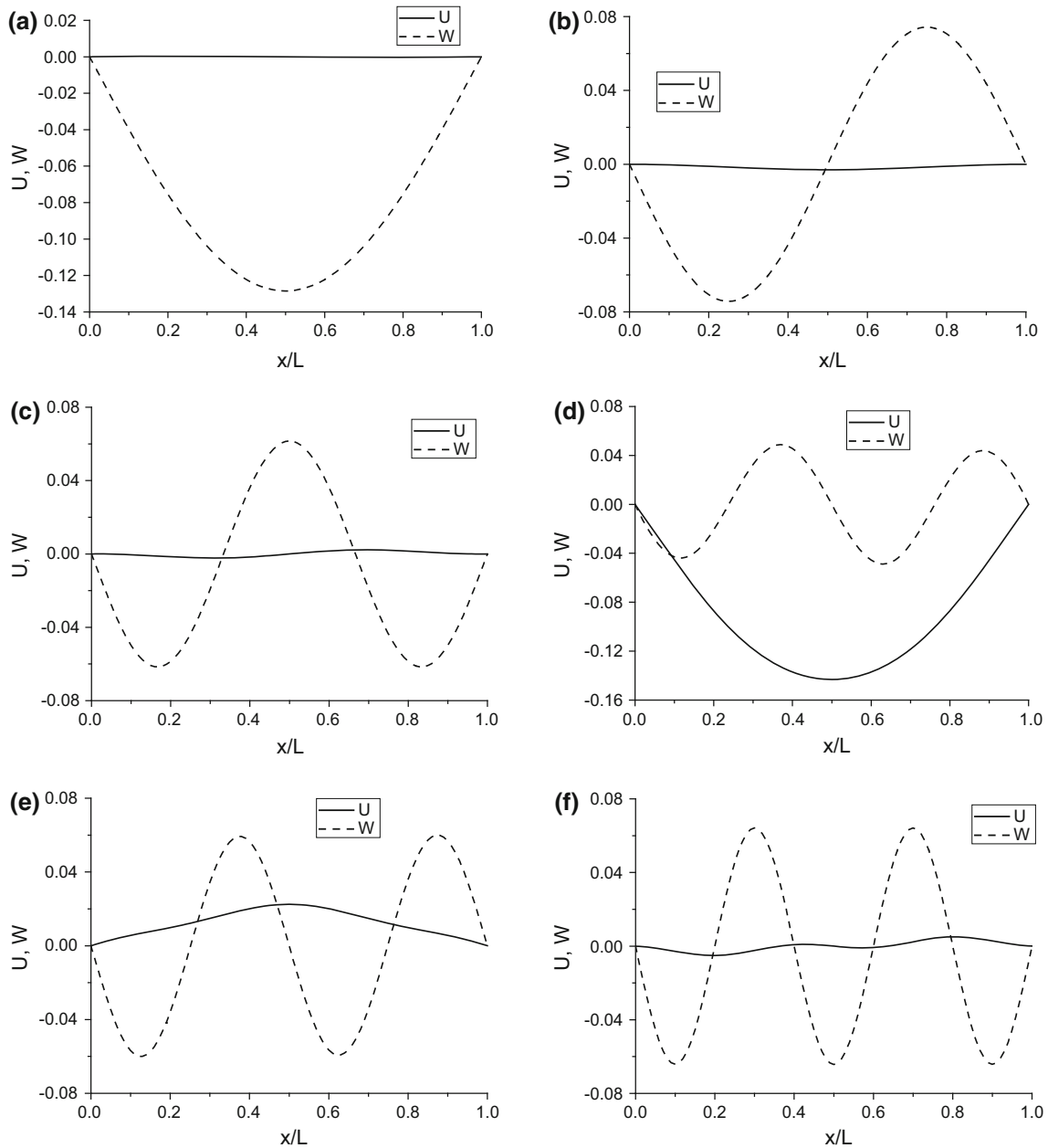


Fig. 7 First six mode shapes of the H–H composite beam with $\Delta T = 780^\circ\text{C}$: **a** mode 1; **b** mode 2; **c** mode 3; **d** mode 4; **e** mode 5; **f** mode 6

To demonstrate the effect of temperature change on the fundamental natural frequency of the composite beam, Fig. 6a–c illustrates the variation of the fundamental natural frequency of the composite beam with the temperature rise for the C–C, C–H and H–H boundary conditions, respectively.

It can be noted from Fig. 6 that the change in the fundamental frequency due to temperature rise is significant. The fundamental frequency monotonically reduces when the temperature rise increases. Finally, the fundamental frequency becomes zero at about $\Delta T = 2752.6$, 1510.7 and 784.3°C for the C–C, C–H and H–H boundary conditions, respectively. At this level of temperature rise, the thermal buckling of the composite beam appears.

The first six mode shapes of the H–H composite beam with $\Delta T = 780^\circ\text{C}$, which is very close to the critical temperature change $\Delta T_{cr} = 784.3^\circ\text{C}$, are plotted in Fig. 7. It may be noted that the first six natural

Table 8 Natural frequencies (in Hz) of composite beam without Poisson effect

Mode no.	$\Delta T = 0^\circ\text{C}$			$\Delta T = 180^\circ\text{C}$			$\Delta T = -180^\circ\text{C}$		
	C-C	C-H	H-H	C-C	C-H	H-H	C-C	C-H	H-H
1	1231.0	937.3	667.0	1179.2	869.7	578.0	1280.3	999.9	745.4
2	2799.0	2532.9	2239.6	2714.4	2442.2	2139.3	2880.9	2620.4	2335.5
3	4663.4	4435.3	4200.3	4552.8	4320.9	4081.1	4771.4	4546.9	4316.2
4	6665.3	6462.4	6250.2	6528.6	6323.8	6109.6	6799.2	6598.0	6387.5
5	7904.4	7876.7	7860.8	7904.4	7873.9	7858.6	7904.5	7878.9	7863.0
6	8748.1	8562.0	8363.9	8585.6	8399.8	8198.1	8907.6	8721.8	8526.5

Table 9 Natural frequencies (in Hz) of composite beam ($E_1 = 69 \times 10^9 \text{Pa}$)

Mode no.	$\Delta T = 0^\circ\text{C}$			$\Delta T = 180^\circ\text{C}$			$\Delta T = -180^\circ\text{C}$		
	C-C	C-H	H-H	C-C	C-H	H-H	C-C	C-H	H-H
1	747.6	534.0	353.8	723.9	501.7	309.6	770.5	564.3	393.0
2	1882.1	1603.1	1326.2	1848.1	1564.9	1282.1	1915.5	1640.5	1368.8
3	3351.8	3053.2	2749.1	3311.7	3010.2	2702.5	3391.4	3095.5	2795.0
4	3940.6	3936.9	3925.1	3940.6	3936.7	3923.9	3940.6	3937.1	3926.1
5	5030.0	4747.5	4460.9	4984.0	4699.6	4411.5	5075.6	4794.9	4509.9
6	6844.0	6582.3	6310.3	6792.0	6529.0	6255.4	6895.6	6635.2	6364.7

frequencies of the H-H composite beam with $\Delta T = 780^\circ\text{C}$ are 28.7, 1216.7, 2718.2, 4239.0, 4499.9, and 6365.0 Hz, respectively.

Figure 7 shows that the axial displacement is coupled with the transverse displacement except for the fundamental mode. The coupling between the axial displacement and the transverse displacement is rather weak for the second the third modes. However, this coupling is rather strong for the fourth mode.

To show the Poisson effect on the natural frequencies of the composite beam, the first six natural frequencies of the composite beam with the Poisson effect ignored for three boundary conditions and three temperature changes (i.e., $\Delta T = 0^\circ\text{C}$, $\Delta T = 180^\circ\text{C}$ and $\Delta T = -180^\circ\text{C}$) are computed and presented in Table 8.

From Tables 6, 7 and 8, the influence of Poisson effect on the natural frequencies of the composite beam can be assessed. It is clear that the natural frequencies obtained with the Poisson effect excluded significantly deviate from the results predicted with the Poisson effect included. For the case of temperature rise ($\Delta T = 180^\circ\text{C}$), it is worthwhile to observe that the maximum percentage differences between the first six natural frequencies obtained with and without the Poisson effect included are about 52.8, 59.3 and 70.2% for the C-C, C-H and H-H boundary conditions, respectively. Also the average differences are about 40.6, 44.9 and 50.2% for the C-C, C-H and H-H boundary conditions, respectively. The results presented in Tables 6, 7 and 8 indicate that the natural frequencies predicted with the Poisson effect ignored have large errors when compared to the results predicted with the Poisson effect included. Therefore, any one-dimensional laminated beam models with the Poisson effect neglected cannot be used to accurately estimate the natural frequency of the composite beams with general laminations.

The effect of material anisotropy on the first six natural frequencies of the composite beam with various boundary conditions is shown in Table 9. It is noted that the value of E_1 is varied from 138×10^9 to 69×10^9 Pa, while the other material properties are kept the same.

Tables 6, 7 and 9 show clearly that the smaller the value of E_1 is, the lower the natural frequency of the composite beam is. For the case of temperature rise ($\Delta T = 180^\circ\text{C}$), altering the value of E_1 from 138×10^9 to 69×10^9 Pa decreases the fundamental frequencies of the composite beam by approximately 7.5, 8.1 and 8.8%, and decreases the sixth natural frequencies of the composite beam by approximately 4.1, 4.4 and 4.9% for the C-C, C-H and H-H boundary conditions, respectively. The natural frequencies of the composite beam for the fundamental modes decrease with faster rate than for the sixth modes.

5 Conclusions

Natural vibration and buckling behaviors of generally laminated composite beams subjected to uniform temperature changes along beam thickness are investigated. The third-order shear deformation beam theory is

adopted and the Poisson effect is included in the one-dimensional beam constitutive equations. The coupled differential equations governing the natural vibration of generally laminated composite beams subject to uniform temperature changes are deduced using the Hamilton's principle. The dynamic stiffness matrix is formulated from the exact analytical solutions of the homogeneous governing equations of motion of generally laminated composite beams. The dynamic stiffness method together with the Wittrick–Williams algorithm is successfully applied to calculate the natural frequencies and critical temperature changes of the composite beams. The proposed mathematical model and solution procedure gives good results for the prediction of critical temperature changes when compared with the available results in literature. A parametric study is presented to determine the influences of boundary conditions, Poisson effect, temperature change, thermal expansion coefficient and material anisotropy on the natural frequencies of the composite beams. This study is useful for the design engineers to choose the ply angle of laminated composite beams to shift the natural frequencies and critical temperature change as desired or to control the vibration and buckling level.

Appendix

The transformed thermal coefficients α_x , α_y and α_{xy} are defined by [28]

$$\alpha_x = \alpha_1 \cos^2 \vartheta + \alpha_2 \sin^2 \vartheta \quad (26)$$

$$\alpha_y = \alpha_2 \cos^2 \vartheta + \alpha_1 \sin^2 \vartheta \quad (27)$$

$$\alpha_{xy} = (\alpha_1 - \alpha_2) \cos \vartheta \sin \vartheta \quad (28)$$

where ϑ is the angle between the fiber direction and the beam axis, α_1 and α_2 are the thermal expansion coefficients along the fiber direction and normal to the fiber direction, respectively.

The transformed reduced stiffness constants \bar{Q}_{ij} ($i, j = 1, 2, 6$) and \bar{Q}_{ij} ($i, j = 4, 5$) are defined by [28]

$$\bar{Q}_{11} = Q_{11} \cos^4 \vartheta + 2(Q_{12} + 2Q_{66}) \sin^2 \vartheta \cos^2 \vartheta + Q_{22} \sin^4 \vartheta \quad (29)$$

$$\bar{Q}_{12} = (Q_{11} + Q_{22} - 4Q_{66}) \sin^2 \vartheta \cos^2 \vartheta + Q_{12}(\sin^4 \vartheta + \cos^4 \vartheta) \quad (30)$$

$$\bar{Q}_{22} = Q_{11} \sin^4 \vartheta + 2(Q_{12} + 2Q_{66}) \sin^2 \vartheta \cos^2 \vartheta + Q_{22} \cos^4 \vartheta \quad (31)$$

$$\bar{Q}_{16} = (Q_{11} - Q_{12} - 2Q_{66}) \sin \vartheta \cos^3 \vartheta + (Q_{12} - Q_{22} + 2Q_{66}) \sin^3 \vartheta \cos \vartheta \quad (32)$$

$$\bar{Q}_{26} = (Q_{11} - Q_{12} - 2Q_{66}) \sin^3 \vartheta \cos \vartheta + (Q_{12} - Q_{22} + 2Q_{66}) \sin \vartheta \cos^3 \vartheta \quad (33)$$

$$\bar{Q}_{66} = (Q_{11} + Q_{22} - 2Q_{12} - 2Q_{66}) \sin^2 \vartheta \cos^2 \vartheta + Q_{66}(\sin^4 \vartheta + \cos^4 \vartheta) \quad (34)$$

$$\bar{Q}_{44} = Q_{44} \cos^2 \vartheta + Q_{55} \sin^2 \vartheta \quad (35)$$

$$\bar{Q}_{45} = (Q_{55} - Q_{44}) \cos \vartheta \sin \vartheta \quad (36)$$

$$\bar{Q}_{55} = Q_{55} \cos^2 \vartheta + Q_{44} \sin^2 \vartheta \quad (37)$$

where the reduced stiffness constants Q_{11} , Q_{12} , Q_{22} , Q_{66} and Q_{44} , Q_{55} can be obtained in terms of the engineering constants [28]

$$Q_{11} = \frac{E_1}{1 - \nu_{12}\nu_{21}} \quad (38)$$

$$Q_{12} = \frac{\nu_{12}E_2}{1 - \nu_{12}\nu_{21}} = \frac{\nu_{21}E_1}{1 - \nu_{12}\nu_{21}} \quad (39)$$

$$Q_{22} = \frac{E_2}{1 - \nu_{12}\nu_{21}} \quad (40)$$

$$Q_{66} = G_{12} \quad (41)$$

$$Q_{44} = G_{23} \quad (42)$$

$$Q_{55} = G_{13} \quad (43)$$

The coefficients η_k ($k = 0 - 4$) appearing in Eq. (17) are

$$\eta_4 = 16(-2\bar{B}_{11}\bar{E}_{11}\bar{F}_{11} + \bar{A}_{11}\bar{F}_{11}^2 + \bar{B}_{11}^2\bar{H}_{11} + \bar{D}_{11}(\bar{E}_{11}^2 - \bar{A}_{11}\bar{H}_{11}))/9h^4 \quad (44)$$

$$\eta_3 = \left(9\bar{A}_{11}\bar{D}_{11}(16\bar{F}_{55} - 8\bar{D}_{55}h^2 + \bar{A}_{55}h^4) + 16\bar{E}_{11}^2\bar{N}_x^T - 24\bar{B}_{11}\bar{E}_{11}h^2\bar{N}_x^T + \bar{A}_{11}(24\bar{F}_{11}h^2 - 9\bar{D}_{11}h^4 - 16\bar{H}_{11})\bar{N}_x^T + 32\bar{B}_{11}(\bar{H}_{11}I_2 - \bar{F}_{11}I_4 - \bar{E}_{11}I_5)\omega^2 + 16(\bar{F}_{11}^2I_1 - \bar{D}_{11}\bar{H}_{11}I_1 - 2\bar{E}_{11}\bar{F}_{11}I_2 + \bar{E}_{11}^2I_3 - \bar{A}_{11}\bar{H}_{11}I_3 + 2\bar{D}_{11}\bar{E}_{11}I_4 + 2\bar{A}_{11}\bar{F}_{11}I_5 - \bar{A}_{11}\bar{D}_{11}I_7)\omega^2 + \bar{B}_{11}^2(-144\bar{F}_{55} + 72\bar{D}_{55}h^2 + 9h^4(-\bar{A}_{55} + \bar{N}_x^T) + 16I_7\omega^2) \right) / (9h^4) \quad (45)$$

$$\eta_2 = \left(9\bar{A}_{11}(16\bar{F}_{55} - 8\bar{D}_{55}h^2 + \bar{A}_{55}h^4)\bar{N}_x^T - 16\bar{E}_{11}^2I_1\omega^2 + (-9\bar{B}_{11}^2h^4I_1 - 8\bar{A}_{11}(3\bar{F}_{11}h^2 - 2\bar{H}_{11})I_1 + 9\bar{A}_{11}(16\bar{F}_{55} - 8\bar{D}_{55}h^2 + \bar{A}_{55}h^4)I_3 + 9\bar{D}_{11}I_1(16\bar{F}_{55} - 8\bar{D}_{55}h^2 + h^4(\bar{A}_{11} + \bar{A}_{55} - \bar{N}_x^T)) + (24\bar{F}_{11}h^2I_1 - 16\bar{H}_{11}I_1 - 24\bar{E}_{11}h^2I_2 - 9\bar{A}_{11}h^4I_3 + 32\bar{E}_{11}I_4 + 24\bar{A}_{11}h^2I_5 - 16\bar{A}_{11}I_7)\bar{N}_x^T + 6\bar{B}_{11}(-48\bar{F}_{55}I_2 + h^2(4\bar{E}_{11}I_1 + 24\bar{D}_{55}I_2 - 3\bar{A}_{55}h^2I_2 + 3h^2I_2\bar{N}_x^T - 4I_4\bar{N}_x^T)) \right) \omega^2 + 16(\bar{H}_{11}(I_2^2 - I_1I_3) - 2\bar{F}_{11}I_2I_4 + 2\bar{E}_{11}I_3I_4 + \bar{D}_{11}I_4^2 + 2\bar{F}_{11}I_1I_5 - 2\bar{E}_{11}I_2I_5 - 2\bar{B}_{11}I_4I_5 + \bar{A}_{11}I_5^2 - (\bar{D}_{11}I_1 - 2\bar{B}_{11}I_2 + \bar{A}_{11}I_3)I_7)\omega^4) / (9h^4) \quad (46)$$

$$\eta_1 = \left(-9(16\bar{F}_{55} - 8\bar{D}_{55}h^2 + \bar{A}_{55}h^4)I_1(\bar{A}_{11} - \bar{N}_x^T)\omega^2 + (-24\bar{F}_{11}h^2I_1^2 + 9\bar{D}_{11}h^4I_1^2 + 16\bar{H}_{11}I_1^2 + 24\bar{E}_{11}h^2I_1I_2 - 18\bar{B}_{11}h^4I_1I_2 - 144\bar{F}_{55}I_2^2 + 72\bar{D}_{55}h^2I_2^2 - 9\bar{A}_{55}h^4I_2^2 + 144\bar{F}_{55}I_1I_3 - 72\bar{D}_{55}h^2I_1I_3 + 9\bar{A}_{11}h^4I_1I_3 + 9\bar{A}_{55}h^4I_1I_3 - 32\bar{E}_{11}I_1I_4 + 24\bar{B}_{11}h^2I_1I_4 - 24\bar{A}_{11}h^2I_1I_5 + 16\bar{A}_{11}I_1I_7 + (9h^4(I_2^2 - I_1I_3) - 24h^2(I_2I_4 - I_1I_5) + 16(I_4^2 - I_1I_7))\bar{N}_x^T)\omega^4 + 16(-2I_2I_4I_5 + I_1I_5^2 + I_2^2I_7 + I_3(I_4^2 - I_1I_7))\omega^6) / (9h^4) \quad (47)$$

$$\eta_0 = (I_1\omega^4(-9(16\bar{F}_{55} - 8\bar{D}_{55}h^2 + \bar{A}_{55}h^4)I_1 + (-9h^4(I_2^2 - I_1I_3) + 24h^2(I_2I_4 - I_1I_5) + 16(-I_4^2 + I_1I_7))\omega^2)) / (9h^4) \quad (48)$$

References

1. Kapania, R.K., Raciti, S.: Recent advances in analysis of laminated beams and plates, part I: shear effects and buckling. *AIAA J.* **27**, 923–934 (1989)
2. Kapania, R.K., Raciti, S.: Recent advances in analysis of laminated beams and plates, part II: vibration and wave propagation. *AIAA J.* **27**, 935–946 (1989)
3. Mathew, T.C., Singh, G., Rao, G.V.: Thermal buckling of cross-ply composite laminates. *Comput. Struct.* **42**, 281–287 (1992)
4. Lan, T., Lin, P.D., Chen, L.W.: Thermal buckling of bimodular sandwich beams. *Compos. Struct.* **25**, 345–352 (1993)
5. Abramovich, H.: Thermal buckling of cross-ply composite laminates using first-order shear deformation theory. *Compos. Struct.* **28**, 201–213 (1994)
6. Mannini, A.: Shear deformation effects on thermal buckling of cross-ply composite laminates. *Compos. Struct.* **39**, 1–10 (1997)
7. Suresh, R., Singh, G., Rao, G.V.: Nonlinear dynamic stability of laminated beams subjected to pulsating thermal loads. *AIAA J.* **37**, 521–524 (1999)
8. Lee, J.J., Choi, S.: Thermal buckling and postbuckling analysis of a laminated composite beam with embedded SMA actuators. *Compos. Struct.* **47**, 695–703 (1999)
9. Khdeir, A.A.: Thermal buckling of cross-ply laminated composite beams. *Acta Mech.* **149**, 201–213 (2001)
10. Aydogdu, M.: Thermal buckling analysis of cross-ply laminated composite beams with general boundary conditions. *Compos. Sci. Technol.* **67**, 1096–1104 (2007)
11. Pradeep, V., Ganesan, N., Bhaskar, K.: Vibration and thermal buckling of composite sandwich beams with viscoelastic core. *Compos. Struct.* **81**, 60–69 (2007)
12. Xiang, H.J., Yang, J.: Free and forced vibration of a laminated FGM Timoshenko beam of variable thickness under heat conduction. *Compos. Part B* **39**, 292–303 (2008)
13. Mahi, A., Adda Bedia, E.A., Tounsi, A., Mechab, I.: An analytical method for temperature-dependent free vibration analysis of functionally graded beams with general boundary conditions. *Compos. Struct.* **92**, 1877–1887 (2010)
14. Wattanasakulpong, N., Prusty, B.G., Kelly, D.W.: Thermal buckling and elastic vibration of third-order shear deformable functionally graded beams. *Int. J. Mech. Sci.* **53**, 734–743 (2011)
15. Kiani, Y., Rezaei, M., Taheri, S., Eslami, M.R.: Thermo-electrical buckling of piezoelectric functionally graded material Timoshenko beams. *Int. J. Mech. Mater. Des.* **7**, 185–197 (2011)
16. Fu, Y., Wang, J., Mao, Y.: Nonlinear analysis of buckling, free vibration and dynamic stability for the piezoelectric functionally graded beams in thermal environment. *Appl. Math. Model.* **36**, 4324–4340 (2012)
17. Vosoughi, A.R., Malekzadeh, P., Banan, M.R., Banan, M.R.: Thermal buckling and postbuckling of laminated composite beams with temperature-dependent properties. *Int. J. Nonlinear Mech.* **47**, 96–102 (2012)

18. Anandrao, K.S., Gupta, R.K., Ramchandran, P., Rao, G.V.: Thermal buckling and free vibration analysis of heated functionally graded material beams. *Def. Sci. J.* **63**, 315–322 (2013)
19. Fu, Y., Wang, J., Hu, S.: Analytical solutions of thermal buckling and postbuckling of symmetric laminated composite beams with various boundary conditions. *Acta Mech.* **225**, 13–29 (2014)
20. Emam, S., Eltaher, M.A.: Buckling and postbuckling of composite beams in hygrothermal environments. *Compos. Struct.* **152**, 665–675 (2016)
21. Reddy, J.N.: *Mechanics of Laminated Composite Plates: Theory and Analysis*. CRC Press, Boca Raton (1997)
22. Leung, A.Y.T.: *Dynamic Stiffness and Substructures*. Springer, London (1993)
23. Banerjee, J.R.: Dynamic stiffness formulation for structural elements: a general approach. *Comput. Struct.* **63**, 101–103 (1997)
24. Lee, U.: *Spectral Element Method in Structural Dynamics*. Inha University Press, Incheon (2004)
25. Wittrick, W.H., Williams, F.W.: A general algorithm for computing natural frequencies of elastic structures. *Q. J. Mech. Appl. Math.* **24**, 263–284 (1971)
26. Li, J., Wang, S., Li, X., Kong, X., Wu, W.: Modeling the coupled bending-torsional vibrations of symmetric laminated composite beams. *Arch. Appl. Mech.* **85**, 991–1007 (2015)
27. Wolfram, S.: *Mathematica: A System for Doing Mathematics by Computer*, 2nd edn. Addison-Wesley, Reading (1991)
28. Jones, R.M.: *Mechanics of Composite Materials*. McGraw-Hill, New York (1976)